

Review on Polymeric, Inorganic, and Composite Materials for Air Filters: From Processing to Properties

Laura M. Henning,* Amanmyrat Abdullayev, Cekdar Vakifahmetoglu, Ulla Simon, Hiba Bensalah, Aleksander Gurlo, and Maged F. Bekheet

Particulate and gaseous air pollutants pose a threat to human health and contribute to climate change. By today, air filters, stationary and portable, are markedly improved and can often provide innocuous air pollution levels. After introducing the classification and standards on air filters, the influence of the processing route and its parameters on the resulting air filter properties and consequently its performance are discussed. Numerous tools are presented to adjust structural properties such as fiber or pore diameter, specific surface area, surface charge, hydrophilicity, or photocatalytic activity to achieve the desired performance in terms of high filtration efficiencies, sufficient mechanical stability, regeneration eligibility, antimicrobial and optical properties. In particular, inorganic and composite materials as well as nonfibrous structures are covered, which are currently holding an outsider position in an air filter community dominated by polymeric materials and fibrous structures.

threat to human health, air pollution is also closely interlinked to climate change and problems associated therewith.^[2] Undoubtedly and above all, it is most desirable to develop and apply techniques generating fewer air pollutants to preserve human and environmental health. Until that is accomplished, and for indoor areas in which sufficient reduction cannot be achieved easily, e.g., airborne pathogens such as the current severe acute respiratory syndrome coronavirus 2 (SARS-CoV-2) provoking the Coronavirus disease 2019 (COVID-19), air filters are a trusted and proven instrument to achieve improved or innocuous air qualities.^[3] Nonmedical cloth face masks, also known as community masks, were found to reduce the transmission of SARS-CoV-2, but do not reach

the performance and protection provided by filtering facepiece respirators.^[4]

In everyday life, air filters are mostly used to filtrate cabin air in vehicles such as cars and airplanes. They are also used in clean rooms and other air-handling installations, for example, in warehouses or laboratories. Other common applications include gas turbines, compressors, and engines. To be used as personal protective equipment, elastic bands are attached to the produced filter material to form surgical or face masks. This is of particular importance for people working in areas potentially harmful to health, such as medical institutions or on construction sites. For special applications or long-time usage, the filter material can be fit into reusable rubber masks, e.g., made from silicone, yielding professional gas masks.


The first modern air-purifying respirator with a filter made of moistened wool was invented by Lewis Haslett, in 1849.^[5] By today, air filtration was already improved significantly with respect to performance, sustainability, and multifunction. A general overview of different air filtration technologies for indoor building ventilation is available.^[6] Furthermore, the progress on particulate matter (PM) filtration and face masks was more recently reviewed, emphasizing different materials and their performance.^[7–9] It becomes apparent that the majority of modern air filters is based on synthetic, polymeric materials. Polymers are most commonly processed into fibrous structures at moderate temperatures by spinning techniques, with electrospinning leading the way. The production of air filters from polymers and biopolymers by the electrospinning process was recently discussed in several review articles.^[10–13] However, polymer-based

1. Introduction

Air pollution causes an estimated seven million premature deaths worldwide every year, i.e., one in every nine deaths, according to the World Health Organization (WHO). More than 80% of people in urban areas, most severely in low- and middle-income countries, are exposed to air pollution levels that exceed WHO guideline limits.^[1] Hence, they suffer elevated risks for cardiovascular and respiratory illnesses. In addition of being a

L. M. Henning, A. Abdullayev, Dr. U. Simon, Dr. H. Bensalah, Prof. A. Gurlo, Dr. M. F. Bekheet
Fachgebiet Keramische Werkstoffe/Chair of Advanced Ceramic Materials, Institut für Werkstoffwissenschaften und -technologien
Fakultät III
Technische Universität Berlin
Hardenbergstr. 40, 10623 Berlin, Germany
E-mail: laura.m.henning@ceramics.tu-berlin.de

Prof. C. Vakifahmetoglu
Department of Materials Science and Engineering
Izmir Institute of Technology
35430 Urla, Izmir, Turkey

 The ORCID identification number(s) for the author(s) of this article can be found under <https://doi.org/10.1002/aesr.202100005>.

© 2021 The Authors. Advanced Energy and Sustainability Research published by Wiley-VCH GmbH. This is an open access article under the terms of the Creative Commons Attribution License, which permits use, distribution and reproduction in any medium, provided the original work is properly cited.

DOI: 10.1002/aesr.202100005

air filters often lack sufficient regeneration options and their single-use does not reflect the spirit of the times. In contrast, inorganic materials such as ceramics and metals are more easily regenerable due to their higher resistance towards elevated temperatures and harsh chemical conditions. Recently, researchers provided insights into the removal of air pollutants by activated carbon (AC) and carbon nanotubes (CNTs).^[14,15] The utilization of inorganic materials, on their own or in the form of composites, and alternative processing techniques open up new possibilities in enhancing modern air filters.

However, previous reviews mainly focused on fibrous structures, polymeric materials, and electrospinning fabrication technology. Less or no attention was paid to the competitive properties of nonfibrous structures, inorganic and composite materials, and other processing routes. Our review aims to fill the gap by giving an overview of processing techniques and filtration mechanisms for both fibrous and nonfibrous air filters composed of polymeric, inorganic, and composite materials. First, the classification of air pollutants and their impact on human beings and the environment will be introduced. Afterward, the mechanisms of air filtration, performance evaluation, and worldwide classification will be elucidated. In the main part of this Review, the latest progress on processing techniques of fibrous, cellular, and granular air filters will be discussed, as shown in **Figure 1**. Emphasis will be put on air filters for room temperature applications and filtration of PM. Processing parameters, possibilities, and limits will be described for polymeric, composite, and inorganic materials. In the following, special attention will be devoted to tailoring structural and material properties to improve the properties and performance of air filters. Additional filter features such as antibacterial properties and filtration of gaseous pollutants will be exploited. All things considered, the reader will be provided with a well-resourced toolbox for air filter understanding and performance optimization, considering sustainability and filter regeneration. Finally, remaining challenges and possible solutions within the progress of air filter research will be addressed.

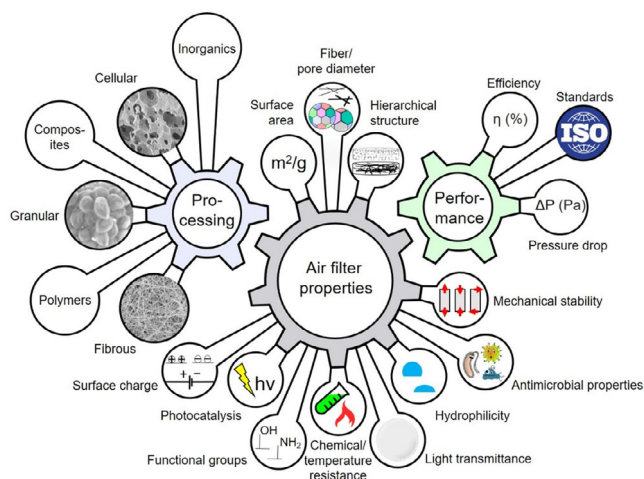


Figure 1. Schematic illustration of this Review showing the dependence of the air filter performance on the air filter properties, which are governed by the choice of material and processing technique.

2. Air Pollutants and Their Impact

A variety of gaseous and particulate substances from both natural and anthropogenic sources can cause air pollution, leading to short- and long-term harm to human and environmental health, as schematically shown in **Figure 2**. Air pollutants can be classified according to their source, chemical composition, size, or release mode. Common classifications are primary versus secondary, indoor versus outdoor, and gaseous versus particulate pollutants.^[16] Primary pollutants such as oxides of sulfur, nitrogen, and carbon, as well as PM from ash, smoke, and dust, are directly emitted into the atmosphere from natural and anthropogenic sources. When primary pollutants react with atmospheric constituents, secondary pollutants such as ground-level ozone, nitrogen oxides, or acid rain are produced.^[17] Air pollutants can also be classified according to the place of emission. For instance, combustion products and volatile organic compounds (VOCs) released from indoor activities, e.g., cooking, smoking, and heating, furniture, building materials, and paint, are called indoor pollutants. In contrast, outdoor pollutants are predominantly generated from power plants, industries, and vehicles, which emit large amounts of various pollutants. However, the most common classification of pollutants is gaseous versus particulate.

The main gaseous pollutants are volatile oxides of nonmetallic elements such as sulfur, nitrogen, and carbon, and VOCs. On the contrary, particulate pollutants or PM refer to the solid particles, liquid droplets, or mixtures of both, including aerosols formed with viruses, bacteria, and spores. PM is usually further subclassified according to the size, denoted as PM_x, whereby *x* describes the maximum particle diameter in micrometer (μm). Established classes are coarse PM₁₀, fine PM_{2.5}, and ultrafine PM_{0.1}. This well-known filterable PM (FPM) is distinguished from condensable particulate matter (CPM).^[18] CPM is gaseous at fuel gas temperature but forms a solid or liquid substance after dilution and cooling, which belongs to harmful PM_{2.5}. Frequent precursors of CPM are VOCs and sulfur oxides.

The UN General Assembly listed air pollution within the five main risks for noncommunicable diseases. The harmful effect of air pollutants on human health strongly depends on the type of

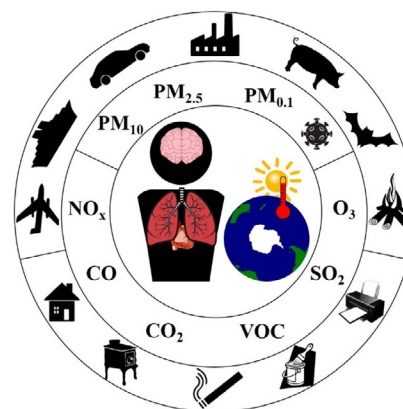


Figure 2. Schematic illustration of the main gaseous and particulate air pollutants produced from selected outdoor and indoor sources and their harmful effects on human and environmental health.

pollutant, its amount, as well as the time of exposure and possible accumulation in the body over time.^[19] It is widely accepted that air pollution causes respiratory diseases such as chronic obstructive pulmonary disease (COPD), asthma, and lung cancer. In that respect, nitrogen dioxide and sulfur dioxide, in particular, were found to be noticeably associated with respiratory diseases and lung cancer mortality, respectively.^[20] Furthermore, acute and chronic cardiovascular diseases such as myocardial ischemia and infarctions, heart failure, and strokes were found to be provoked by air pollutants, predominantly by fine PM_{2.5} and ultra-fine PM_{0.1}.^[21]

The PM inhaled into the pulmonary tree may harm the human body via: i) instigation of systemic inflammation and/or oxidative stress, ii) alterations in autonomic balance, and iii) direct actions upon the vasculature of particle constituents. Other than that, pathogens such as influenza or SARS viruses can spread by airborne or aerosol transmission, followed by disease outbreaks.^[22] Without protection using air filters or other means, outbreaks can possibly evolve into pandemics and endanger the health and life of millions of people. Examples include the 1918 influenza pandemic, also known as Spanish flu, or the current COVID-19 pandemic.

Air pollution does not only cause harm to human health, but also to the environment. Major damaging effects include i) acid rain, which acidifies water and soil environments, ii) haze from PM dispersed in air, iii) ozone thinning in Earth's protective stratospheric layer, and iv) climate change, including global warming induced by elevated emission of greenhouse pollutants, such as carbon and nitrogen oxides and methane.^[23] In addition, climate change is expected to exacerbate further human health impacts by increasing weather conditions that enhance air pollution exposure, mainly to PM_{2.5} and ozone.^[24,25] To break the cycle of air pollution and climate change, air pollution needs to be restricted more drastically. In this regard, air filters provide a suitable method for air purification.

3. Fundamental Principles of Air Filters

In the following section, the mechanisms of air filtration of particulate and gaseous pollutants will be introduced. Furthermore, key factors in the evaluation of air filter performance will be

presented. An overview of the worldwide classification and standardization of air filters according to these key factors will be provided. Furthermore, the influence of the model pollutant on the air filter performance will be discussed.

3.1. Mechanisms of Air Filtration

Particulate and gaseous adsorbents significantly differ in size and chemical composition. Thus, they behave differently within the air flow and require different approaches for removal. In the following, the underlying mechanisms for the removal of particulate and gaseous pollutants will be elucidated.

3.1.1. Filtration of Particulate Pollutants

Several mechanisms were reported to be involved in the filtration of PM, as shown in **Figure 3a,b**, namely sieving, gravity settling, inertial impaction, interception, diffusion, and electrostatic attraction.^[26,27]

Sieving takes place when the particles are too large to enter the pores of the filters and are retained on the barrier. As sieving requires adequately small pore sizes, usually in the range of 3–8 nm,^[28,29] the corresponding pressure drop is commonly in the range of a few hundreds or thousands of Pa. This is much higher than that of other mechanisms, making sieving hardly competitive as the main filtration mechanism for air filters, compare Section 4.

Particles larger than 5 μm experience a significant net downward motion and can be filtered by gravity settling. This mechanism is barely relevant for common air filters as such particles often settle before reaching the filter surface. In contrast, small particles with high inertia that can enter the filter material have sufficient momentum to break away from the air streamline and collide with the filter medium, being separated by impaction. Thus, this mechanism is called inertial impaction. In case the particles do not have sufficient inertia to depart from the gas streamline, they can still be filtered by collision with the filter medium, i.e., by interception mechanism. Both inertial impaction and interception mechanisms are more likely to occur with higher internal tortuosity of the filter medium and are among the most common filter mechanisms, especially for fibrous filters.

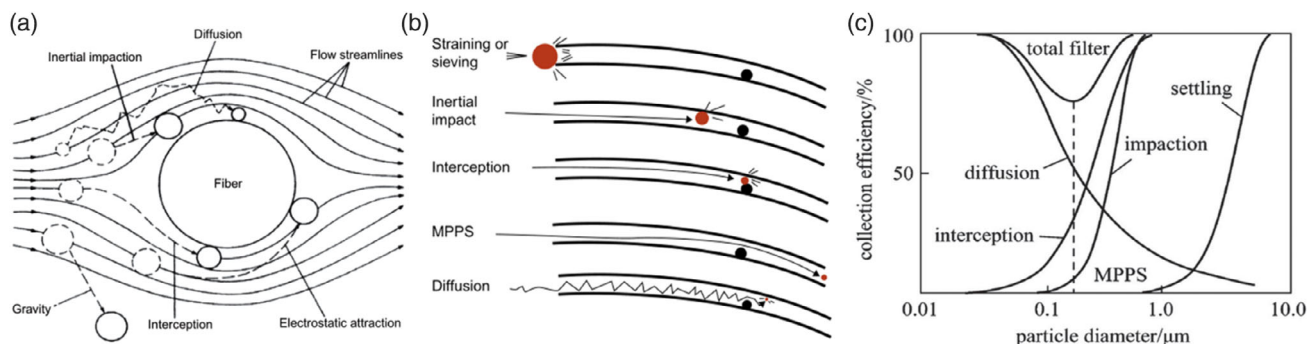


Figure 3. Schematic representation of the major filter mechanisms sieving, gravity settling, inertial impaction, interception, diffusion, and electrostatic attraction for particle matter a) past a single fiber and b) through a pore. Reproduced with permission.^[26] Copyright (2016), Elsevier. MPPS describes the most penetrating particle size for which a filter is least effective. c) Dependence of the particle size on the major filter mechanisms and the resulting total filter efficiency, Reproduced with permission.^[230] Copyright 2012, John Wiley and Sons.

The exploitation of these mechanisms comes along with low pressure drop values, mostly below 100 Pa, compare Section 4.

Diffusion is based on the Brownian motion and migration of particles smaller than 0.5 μm within the gaseous medium with concentration gradients of particles from the regions of higher concentration to those of lower local concentration, i.e., to the surface of the filter medium. Electrostatic attraction, based on the surface electrical charge of the particle and/ or fiber medium, causes particles to divert from the streamline and settle on the fiber medium. The electrical field can also be externally imposed. Electrostatic pollutant capture emerged as the most frequently applied filtration mechanism, as it conveniently allows to obtain pressure drop values below 50 Pa down to values as low as 0–0.5 Pa, compare Section 5. Still, there usually exist particles small enough to stay with the streamline, regardless of wall surfaces or other obstacles. As a result, those cannot be withheld by the filter medium. Among that, as shown in Figure 3c, different mechanisms are dominant for different particle sizes. As a result, for each filter, there exists a particle size, for which filters are least effective, called the most penetrating particle size (MPPS). The MPPS usually is in the particle size range of 0.04–0.4 μm . Research emphasis is mostly focused on removing the particles within this size range, as they are hard to remove and might pose a serious health threat due to their ability to enter the lower respiratory tract.

In addition to the methods mentioned earlier, adsorption is often proposed as one of the underlying filtration mechanisms, not specifying the exact nature of pollutant adhesion, compare Section 4. As adsorption occurs at the surface, the available surface area of the filter material is of most importance. In addition, adsorption can be significantly enhanced by functional surface groups.^[30–32]

3.1.2. Filtration of Gaseous Pollutants

Chemical air filters, also called air purifiers, can be applied to remove gaseous pollutants from the air via physisorption, and/or chemisorption.^[33] Physisorption is based on weak van der Waals forces between the filter material and the pollutant. van der Waals bonds are comparably weak, whereas a strong bond between the filter material and pollutant can be formed during chemisorption. Hence, molecules bond by physical adsorption can migrate about the surface and be easily removed from the filter surface during regeneration. In contrast, molecules bond by chemical sorption are restricted to specific surface sites and can hardly be removed by reasonable energy demands.

3.2. Performance Evaluation

3.2.1. Model Pollutants

When determining the performance of an air filter, the size of the model pollutant is not the only important factor to consider, but so is its shape, surface charge, or ability to form stable aerosols. Air filter performance factors are most commonly determined using NaCl as a model pollutant because it forms cubic particles with round edges. Furthermore, it is a low-cost material, which is easy to handle and easily available. NaCl is well

suitable to average filtration efficiencies considering that spherical particles like spherical polystyrene latex result in higher filtration efficiency compared with cubic particles like MgO of the same aerodynamic size.^[34] Incense smoke is another commonly used model pollutant, which produces particles mostly smaller than 2.5 μm as well as gas products like CO, CO₂, NO₂, SO₂, and VOCs such as benzene, toluene, xylenes, aldehydes, and polycyclic aromatic hydrocarbons.^[35] Thus, incense smoke exhibits both polar functional groups such as C–O, C=O, and C–N, and nonpolar functional groups like C–C, C–H, and C=C.^[36] To represent organic matter and oil droplets, di-ethyl-hexyl-sebacat (DEHS) is a frequently used model pollutant as it forms a stable aerosol.^[37] Depending on the temperature and relative humidity, changes in the morphology or state of the test pollutants may occur and should be considered.^[38] Recently, a low-cost optical measurement for testing the efficacy of facemasks against expelled droplets during the speech was presented and applied to commercial masks and mask alternatives such as neck fleece and bandanas.^[39]

The evaluation of antimicrobial properties is usually ascertained by aerosol filtration and subsequent cell incubation or in liquid media, which can be problematic due to safety concerns. Instead, testing in liquid media can be carried out. Recently, researchers presented a novel method of determining the antiviral performance of air filters against airborne infectious viruses. This allows deriving results for tests in an air medium from tests in a liquid medium without the need for aerosolized viruses.^[40]

3.2.2. Key Performance Indicators

The removal or filtration efficiency η , which is one of the most important factors to evaluate the performance of any filter, is defined as the percentage of contaminant removed by the filter, according to Equation (1), where c_0 and c_1 ($\mu\text{g m}^{-3}$) are the upstream and downstream concentrations of the contaminant, respectively.

$$\eta(\%) = \frac{(c_0 - c_1)}{c_0} \times 100 \quad (1)$$

In contrast to the filtration efficiency, which should be as high as possible, the pressure drop ΔP , which represents the pressure loss through the filter, should be remained as small as possible. This reduces both energy demand and breathing resistance. The pressure drop ΔP (Pa) is practically determined by measuring the difference between upstream and downstream pressure P_0 and P_1 (Pa), respectively, according to Equation (2).

$$\Delta P = P_0 - P_1 \quad (2)$$

The pressure drop ΔP (Pa) can be expressed by Darcy's law, according to Equation (3), where h , μ , U , and k are the filter thickness (m), gas viscosity (Pa s), gas velocity at the surface of the filter (m s^{-1}), and permeability (m^2), respectively. As shown in Equation (3), Darcy's model represents a linear relationship between the pressure drop and the gas velocity in porous media. Accordingly, the gas velocity should be considered when comparing the pressure drop values of different air filters. However, in some cases, especially at high gas velocities and for complex pore

structures, deviations from Darcy's model can be observed. Thus, other models, such as the Forchheimer model, can be used to correlate this nonlinear relationship between pressure drop and the gas velocity based on inertial effects.^[41] The Forchheimer model extends Darcy's linear law by an additional quadratic term $\beta\rho U^2$, where β represents the inertial coefficient (m^{-1}) and ρ is the air density (kg m^{-3}), to account for the change in pressure drop.^[42] The Forchheimer number, which refers to the ratio between the viscous and inertial effects, can be used as criterion to decide for the applicability of the respective models.^[43]

$$\frac{\Delta P}{h} = \frac{\mu U}{k} \quad (3)$$

Finally, the overall filtration performance of a filter can be evaluated by calculating the quality factor, QF, according to Equation (4), considering both efficiency and pressure drop factors. Thus, the QF is considered as a benefit-to-cost ratio.

$$\text{QF} = \frac{-\ln(1 - \eta)}{\Delta P} \quad (4)$$

3.3. Classification and Standardization of Air Filters

Air filters can be classified according to their performance, application, operation principle, or material composition. Commonly, air filters are classified according to their efficiency based on regulations published by international organizations such as the International Organization for Standardization (ISO), regional organizations such as the European Committee for Standardization (Comité Européen de Normalisation, CEN), Europe's Industry Association for Indoor Climate (HVAC), Process Cooling, and Food Cold Chain Technologies (EUROVENT), or national organizations such as the American Society for Testing and Materials (ASTM), American Society of Heating, Refrigeration and Air Conditioning Engineers (ASHRAE), and from the China Association for Standardization (CAS) and China Household Electric Appliance Research Institute (CHEARI), among others. These organizations do not only classify air filters, but also recommend widely accepted regulations for air filter testing.

For instance, according to the European standard EN 1822, from which the current international standard ISO 29463 was derived, air filters are classified as efficient particulate air (EPA) filters with efficiencies of 85–99.5%, high-efficiency particulate air (HEPA) filters with efficiencies of 99.95–99.995%, and ultralow penetration air (ULPA) filters with efficiencies of 99.9995–99.999995%. Air filters are commonly tested with particle sizes of 0.3–0.5 μm . Concerning filtering respirators, the European filtering face piece (FFP) classification and the U.S. National Institute for Occupational Safety and Health (NIOSH)'s air filtration rating are well-established standards. The European standard EN 149 describes filtering half masks labeled as FFP1, FFP2, and FFP3, which filter at least 80%, 94%, and 99% of the test pollutants. Tests are conducted with NaCl particles of 0.02–2 μm , having a mean diameter of 0.6 μm and a concentration of $8 \pm 4 \text{ mg m}^{-3}$, as well as with

paraffin oil, at 95 L min^{-1} . The breathing the resistance may not exceed 210, 240, and 300 Pa for FFP1, FFP2, and FFP3 filtering half masks, respectively, for the flow rate given. In the U.S., as governed by Part 84 of Title 42 of the Code of Federal Regulations (CFR), minimum efficiency levels of 95%, 99%, and 99.97% for particles $\geq 0.3 \mu\text{m}$, made from NaCl or oily diethylphthalate (DOP), are assigned to respirator classes X95, X99, and X100, respectively. Thereby, X is replaced with N for respirators not resistant to oil, i.e., particular filtration only, R for respirators resistant to oil, and P for oil-proof and reusable respirators. More recently, the People's Republic of China updated the national standard GB 2626 for respiratory protection, whose effective date was postponed to July 2021 by the Standardization Administration of China (SAC) due to the COVID-19 pandemic to ensure stable respiratory production. The classification contains the filter categories KN for nonoily particles and KP for oily and nonoily particles with the suffix 90, 95, or 100 that refer to the filter efficiencies.

4. Processing Technologies and Performance of Fibrous Air Filters

4.1. Electrospinning

Electrospinning is a commonly used technique to produce fibers and fiber-based meshes by applying a high voltage to a polymeric solution or melt, as shown in **Figure 4a**. During the electrospinning process, the solution becomes electrically charged and overcomes its surface tension, forming a Taylor cone at the needle tip, which is subsequently stretched in a jet form toward a grounded plate or rotary collector. On its way to the collector, the jet dries, and the present solvent evaporates, resulting in fibers having diameters in the range of tens to a few hundred nanometers.^[12] Electrospinning allows for the production of continuous fiber assemblies such as nonwoven, aligned, and patterned fiber meshes, as well as random 3D structures, evolved from a long fiber overlaying on itself multiple times.^[44] Exemplary structures for polymeric, inorganic, composite, and metallized fiber structures are shown in **Figure 4b-i**.

Common polymeric building blocks for electrospinning include polyacrylonitrile (PAN), polyvinylidene fluoride (PVDF), polyurethane (PU), polylactic acid (PLA), polybenzimidazole (PBI), polyamide (PA), poly(methyl methacrylate) (PMMA), polydimethylsiloxane (PDMS), and mixtures thereof.^[45–54] However, natural materials, including silk, wool, cellulose, soy protein, gelatin, and chitosan, took on greater significance due to increasing awareness for sustainability.^[13,55–60] Furthermore, expanded polystyrene (EPS) waste was successfully used for the production of air filters by electrospinning.^[61] In addition to the material type and additives, which can be used to functionalize the formed fibers,^[12] process variables such as applied voltage, flow rate, type of collector, and distance between needle tip and collector were adjusted to tailor the final fiber properties such as diameter, length, porosity, pore size, and morphology.^[62] For instance, uniform polymeric PBI nanofiber filters were obtained by electrospinning with a single solvent, see **Figure 4b**,^[51] whereas the usage of a mixed solvent system allows producing polymer-rich and polymer-lean phases within

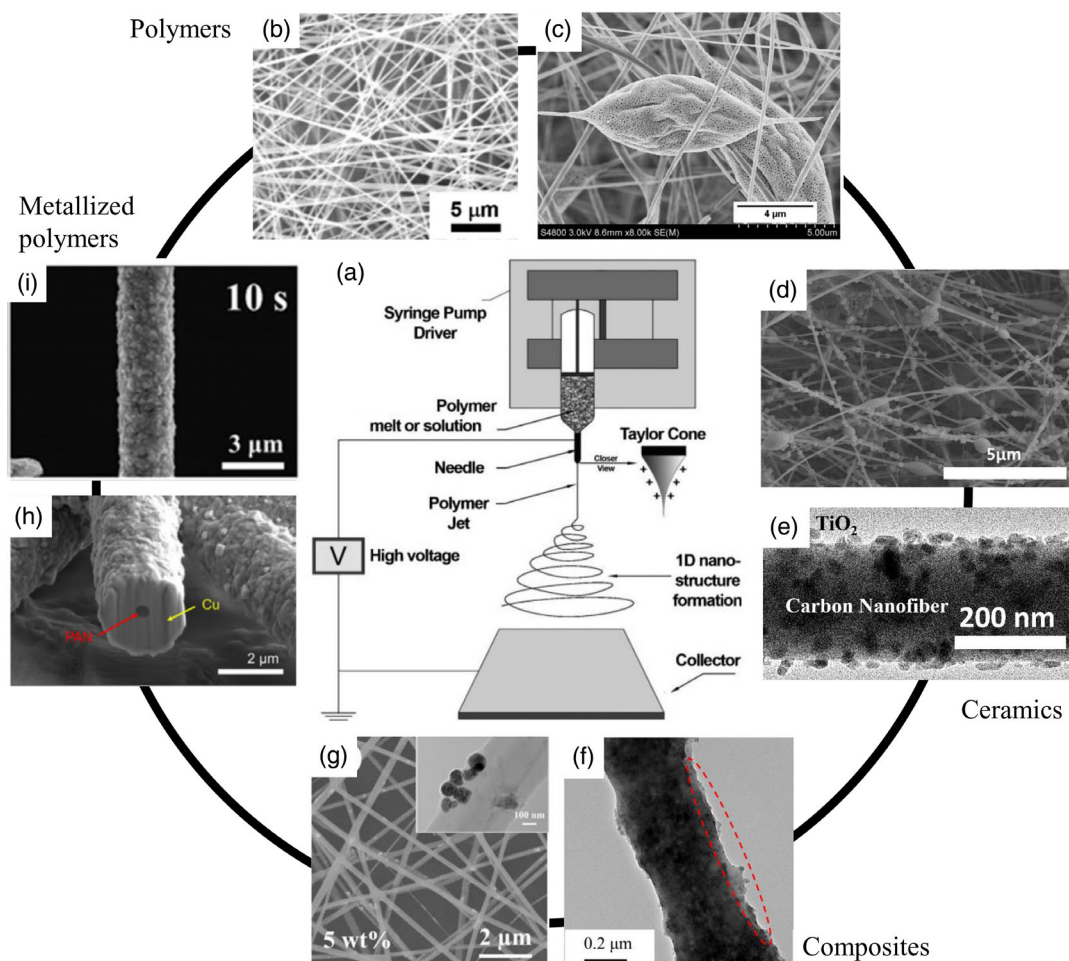


Figure 4. Schematic representation of the a) electrospinning process;^[231] b,c,d,g,h,i) scanning electron microscopy (SEM) and e,f) transmission electron microscopy (TEM) images of electrospun air filter structures made from polymeric b) uniform PBI nanofibers^[51] and c) porous bead-on-string PLA fibers,^[49] ceramic d) ZIF-8 nanocrystals on SiO₂ fibers^[80] and e) TiO₂ NP-decorated carbon nanofibers,^[83] composite f) PVA–PAA fibers with 4 wt% SiO₂ and silver NPs from 0.3 wt% AgNO₃^[37] and g) PU/PSA nanofibers with 5 wt.% BaTiO₃ NPs, inset showing the ceramic NPs in higher resolution,^[64] and h,i) metallized Cu-plated polymeric PAN nanofibers exhibiting a small PAN core and generous copper coating.^[84,85] a) Adapted with permission.^[231] Copyright 2020, Taylor & Francis Group. b) Reproduced with permission.^[51] Copyright 2019, American Chemical Society. c) Reproduced with permission.^[49] Copyright 2015, Elsevier. d) Reproduced with permission.^[80] Copyright 2019, Elsevier. e) Reproduced with permission.^[83] Copyright 2020, Elsevier. f) Reproduced with permission.^[37] Copyright 2018, Elsevier. g) Reproduced with permission.^[64] Copyright 2020, Elsevier. h) Reproduced with permission.^[84] Copyright 2020, American Chemical Society. i) Reproduced with permission.^[85] Copyright 2019, American Chemical Society.

the fiber, resulting in porous bead-on-string PLA fiber filters, as shown in Figure 4c.^[49] Fiber diameters of electrospun polymeric air filters are most commonly in the range of a few hundred nanometers, as shown in Table 1. More recently, a modified bipolar electrospinning technique without a collecting electrode, in which two jets of opposite polarity are used to neutralize each other on an insulating mesh, was applied to produce fibrous air filters.^[63]

As shown in Table 1, several inorganic nanoparticles (NPs) such as TiO₂, SiO₂, Al₂O₃, BaTiO₃, and Fe₃O₄ were recently incorporated into the nanofibers during the electrospinning process to (i) reduce the fiber diameter and pore size, (ii) increase the porosity, surface roughness, and fiber strength, (iii) construct hierarchical structures, and (iv) release negative ions.^[37,64–69] For instance, PVA-PAA-SiO₂-Ag composite fiber filters were

produced by one-step electrospinning of a suspension containing poly(vinyl alcohol) (PVA), poly(acrylic acid) (PAA), SiO₂ NPs, and AgNO₃, whereas the latter two were used to decrease the fiber diameter and generate antibacterial silver NPs, respectively, as shown in Figure 4f.^[37]

Electrospinning of BaTiO₃ NPs in a PU/pressure-sensitive adhesive (PSA) solution yielded composite fibrous filters, which have a rough fiber surface and, thus, increased the surface area for enhanced pollutant capture, see Figure 4g.^[64] However, there remain process-related limits for incorporating inorganic NPs in the electrospinning process as the NPs change the conductivity of the solution and significantly increase its viscosity. For instance, not more than 8% Al₂O₃ could be incorporated in 15% PVDF solution to maintain solution spinnability.^[67] Carbonaceous inorganic materials such as graphene oxide (GO), AC, or CNTs were

Table 1. List of techniques, materials, and observed air filtration properties for selected fibrous air filters produced by electrospinning.

Product ^(a)	Filter characteristics f ϕ = fiber ϕ [nm]	Pollutant/ size [μ m]	Max. removal efficiency [%]	Airflow/ velocity [m s ⁻¹]	Pressure drop [Pa]	QF [Pa ⁻¹]	Dominant filter mechanism(s)
Polymer							
PAN nanofiber air filter laminated on nonwoven support ^[45]	f ϕ 200–300	NaCl 0.3	95	0.05	245	N/A	N/A
PAN nanofibrous membrane ^[46]	f ϕ 77	Cigarette smoke 2.5	99.3	3	N/A	N/A	Inertial impaction, interception, diffusion, gravity settling, electrostatic capture
PVDF self-polarized nanofiber/net filter ^[47]	f ϕ 21, pore size 0.26 μ m	NaCl 0.3	99.998	0.05	93	0.11	Sieving, interception, adhesion
PU electrostatic air filter on mesh substrate ^[48]	f ϕ 140–820	Cigarette smoke < 1	98.9	0.1 L min ⁻¹	10	0.45	Electrostatic capture
PLA porous bead on string membrane ^[49]	f ϕ 144–940, porosity 75–87%	NaCl 0.26	99.997	0.06	165	0.06	Interception, adsorption
PAN bead on string air filter on nonwoven support ^[50]	f ϕ 70–750	NaCl 0.3 paraffin oil aerosol 0.3	99	0.04	27	0.2	Diffusion, electrostatic capture, interception, inertial impaction, gravity settling
Laminated PBI and Nylon-6 nanofiber membrane filter on PE mesh ^[51]	f ϕ 50–650	KCl Diocetyl phthalate (DOP)	98.5 90.2	0.35	131	0.03 0.02	Electrostatic capture
Dual-network PAN nanofiber net membrane on nonwoven substrate ^[52]	f ϕ 630–1350, porosity 83.0–93.9%	NaCl 0.3–10	99.998	0.05	110	0.1	Sieving, interception
Gelatin protein nanofabric filter ^[55]	f ϕ 69–473	Cigarette smoke 0.3–10	99.2	0.05	200	0.03	Sieving, hydrogen bonding, ionic bonding, electrostatic capture
PVA/soy protein nanofabric filter ^[56]	f ϕ 100–200	Cigarette smoke 2.5 10	99.8 99.99	0.05	215	0.03	Sieving, polar bonding, hydrogen bonding, electrostatic capture
Cellulose acetate/poly (ionic liquid) composite air filter ^[57]	f ϕ 399–680	Sandalwood smoke 2.5 10 <i>E. coli</i> , <i>S. aureus</i>	97.9 99.7 100	N/A	N/A	N/A	Adsorption + contact killing
Polymeric composites							
PVA–PAA–SiO ₂ –Ag membrane on nonwoven substrate ^[37]	f ϕ 300–500	DEHS oil 0.3–0.5 NaCl 0.3–0.5 <i>E. coli</i> , <i>Bacillus subtilis</i>	98.0 98.9	32 L min ⁻¹	150	0.03	N/A ZOI 14 mm
PAN-co-PMA:TiO ₂ nanofiber membranes between PP nonwovens ^[65]	f ϕ 400–800	N/A 2.5	99.99	N/A	200	N/A	Electrostatic capture
PET/SiO ₂ composite needle felt on hot melt adhesive film ^[66]	f ϕ 135–350	Al ₂ O ₃ 6.2	99.9	0.5	130	N/A	Electrostatic capture
PVDF–Ag–Al ₂ O ₃ nanofibrous membrane ^[67]	f ϕ 420–1850	DEHS oil 0.36 <i>E. coli</i>	99.2 99.7	0.3	211	N/A	N/A
PVDF/Fe ₃ O ₄ membrane bond on glass fiber/ PET mesh ^[68]	Pore size 1.5–3.5 μ m	NaCl 0.3	99.95	14 L min ⁻¹	59	0.13	Electrostatic capture
BaTiO ₃ @ PU/PSA nanofiber membrane on nonwoven fabric or wire mesh ^[64]	f ϕ 160–248	DEHS oil 0.3 Incense smoke 2.5	99.99	2	68	0.14	Electrostatic capture, interception
GO/ PAN nanofibrous membrane on nonwoven substrate ^[70]	f ϕ 90–300	NaCl 2.5	99.97	0.5	8	1.03	Adsorption

Table 1. Continued.

Product ^{a)}	Filter characteristics f \varnothing = fiber \varnothing [nm]	Pollutant/ size [μ m]	Max. removal efficiency [%]	Airflow/ velocity [m s ⁻¹]	Pressure drop [Pa]	QF [Pa ⁻¹]	Dominant filter mechanism(s)
Soy protein/AC/PVA membrane on PP nonwoven ^[71]	f \varnothing 25–30	NaCl 0.3–7	80	0.05	N/A	N/A	Electrostatic capture, adsorption
PI/PEI/CNT hybrid filter ^[72]	f \varnothing 150–900	Particles 0.3–0.5	99.99	0.05	120	0.08	Interception, diffusion
PAN/PS/ZIF-8 multilayer fibrous membrane ^[74]	f \varnothing 305–1250	DEHS oil 0.3 Incense smoke 0.1–2.5	99.9 99.998	0.05	80	0.1	Adsorption
PVA/Cu nanofibrous air filter on cellulose acetate support ^[76]	f \varnothing 139–1042	KCl 0.5–2 5 <i>E. coli</i>	99.99 99.7 ZOI 1.2 mm	0.05	500	0.16	Impaction, interception + contact killing by disruption of metabolic processes
PU/Ag/AC nano air filter on PP nonwoven ^[77]	f \varnothing 300–700	NaCl 0.3 <i>E. coli</i> , <i>S. aureus</i>	84 ZOI 20 mm	N/A	4	0.47	Sieving, interception, diffusion, inertial impaction + cell membrane damage
Inorganic composites							
ZIF-8@SiO ₂ nanofiber membrane ^[80]	Pore size 10.3 μ m	Incense smoke	99.96	0.02	500–1400	N/A	Electrostatic capture, interception
Ag@SiO ₂ -TiO ₂ flexible nanofibrous membrane on stainless steel mesh ^[81]	f \varnothing 200–300	Incense smoke 2.5 <i>E. coli</i>	99.84 95.8 ZOI 15 mm	0.02	59	N/A	Electrostatic capture + disruption of bacterial respiratory chain and cell damage
Pt/Al ₂ O ₃ flexible nanofibrous membrane ^[82]	f \varnothing 300–400	DOP 0.3	99.97	30 L min ⁻¹	339	N/A	N/A
TiO ₂ @carbon flexible nanofiber membrane ^[83]	f \varnothing 150–300	Cigarette smoke 2.5	99.92	20 L min ⁻¹	63	0.113	Electrostatic capture, interception
Cu-plated nanofiber filter ^[85]	f \varnothing 530–4770, porosity 49–82%	Incense smoke and charcoal powder	79	N/A	N/A	N/A	Electrostatic capture

^{a)}N/A: not available. ZOI: zone of inhibition: diameter of the zone of growth inhibition around the test sample (\varnothing 6–10 mm) in disc diffusion test.

also incorporated in the electrospinning process, resulting in a comparable decrease in fiber diameter.^[70–72] Conductive GO could promote the rearrangement of polymer chains and form olive-like beads on the nanofibers, improving their crystallinity, densification degree, and mechanical properties and the specific area.^[70] Although CNTs are popular for their small fiber diameters and high mechanical strength, they can also be dangerous to human health if they break loose from the fiber network.^[73] Thus, CNT-containing layers are usually bonded, e.g., thermally, when using them for air filter applications.^[72] Other than that, metal–organic frameworks (MOFs), such as ZIF-8 and ZIF-67, were successfully integrated into electrospun fibers by adding them into the electrospinning solution.^[74,75] Antimicrobial metal NPs, such as silver or copper, were successfully incorporated into the filter structure by the addition of metal nitrates or metal acetates into the electrospinning solution, followed by the photo-reduction of electrospun fibers by means of ultraviolet (UV) light.^[37,67,76,77] However, to avoid the increase in the conductivity within the electrospun jet due to the inclusion of a metal salt, immobilization can be performed, e.g., by means of sol–gel crosslinking.^[76]

Several inorganic fibers were fabricated by thermal treatment of electrospun precursors prepared from polymeric solutions.^[78,79] Although the thermal treatment of electrospun precursors is usually carried out under ambient air to decompose organic components, inert atmospheres were also applied to preserve carbon species in the fibers. For instance, calcination of electrospun silica gel, which was produced by sol–gel synthesis utilizing tetraethoxysilane (TEOS) as silica source with PVA, resulted in SiO₂ nanofiber membranes upon calcination at 800 °C, on which porous ZIF-8 nanocrystals could be grown by controlled crystallization to enhance the surface area, as shown in Figure 4d.^[80] Similarly, TEOS and titanium(III) chloride were electrospun as ceramic precursors in ethanol, yielding SiO₂-TiO₂ membranes after calcination. Such membranes were furthermore impregnated by silver via precipitation from AgNO₃ solution.^[81]

Metal–ceramic composite nanofibrous membranes, e.g., from platinum/Al₂O₃, were also produced in a one-pot electrospinning process. The metal and alumina precursors were electrospun and calcined, simultaneously burning the organics, yielding Al₂O₃, and reducing hexachloroplatinate to metallic platinum NPs.^[82]

Furthermore, carbon nanofiber membranes, optionally decorated with TiO₂ NPs, as shown in Figure 4e, could be directly obtained by electrospinning solutions of polyvinylpyrrolidone (PVP) and tetrabutyl titanate as precursors and subsequent pyrolysis, yielding flexible Schottky-junction nanofiber filters, allowing for photoexcitation processes.^[83] Polymeric electrospun fibers can also be metallized, for example, by electroplating, yielding polymer–metal core–shell structures, as shown in Figure 4h,i.^[84,85] In the process, electrospun PAN nanofibers were sputtered with platinum to generate minimal conductivity and subsequently coated with copper by applying a voltage between the sample and a copper electrode inside a copper-based electroplating solution.

Electrospinning is one of the most versatile and commonly used methods to produce modern 1D fibers and fiber meshes for air filter parts. Meanwhile, more researchers are focusing on green electrospinning, in which the polymers and their additives are biocompatible, and mostly hazardous organic solvents are replaced by greener alternatives. Thereby, fibers electrospun in water would be unstable on their own, but can be subsequently crosslinked using either chemical crosslinkers, which are often harmful, or more environmentally friendly physical crosslinking methods such as thermal crosslinking.^[37]

As shown in Table 1, electrospun air filters show very high filtration efficiencies, often exceeding 99%. The majority of coarse and fine PM, nonoily, and oily pollutants, could be removed at pressure drops ranging from single-digit values up to a few hundred Pa, remaining within the breathing resistance limit required for FFP masks. The lowest pressure drops, accompanied by the highest QFs, were achieved by polymeric-inorganic composite air filters, such as GO/PAN nanofibrous membrane filters and PU/Ag/AC nano air filters. Although various filter mechanisms were reported to be exploited for electrospun air filters, mainly electrostatic capture, interception, and adsorption

were found to be utilized. In addition, several electrospun air filter materials, in particular, those containing metal NPs, could successfully inhibit bacterial growth and provoke bacteria death, most commonly represented by the zone of inhibition (ZOI). However, the remarkable performance of electrospun air filters must be balanced against their high production efforts and upscaling potentials for applications beyond laboratory-scale research.

4.2. Melt spinning and Melt Blowing

Melt spinning and melt blowing are among the most frequently utilized techniques to form micrometer-sized nonwoven fiber meshes.^[86] Both techniques are based on melt-extrusion, whereby a molten polymer is extruded through one or several small orifices. For the melt blowing technique, the molten polymer is additionally stretched by a high-speed hot air jet. The polymeric fibers are then collected on a collector as nonwoven webs at a high production rate. As no solvents are required, both can be considered as economically and ecologically feasible methods.^[87] The adaption of the air flow is a powerful tool in tailoring the nonwoven web properties for the melt blowing approach, for which different die geometries such as slot die or annular die can be utilized. The average fiber diameter of the resulting product can be varied between 300 nm and 10 μm^[88,89] or even more, see Table 2, which is considerably larger than the fibers produced by electrospinning.

While initially mostly polyolefins were used as raw materials for melt spinning and melt blowing,^[90–92] recently, also biodegradable and biocompatible polymers such as PLA were also used to produce fabrics for air filter applications.^[93] Melt spinning, followed by collecting the continuous filaments, and binding the filaments in the webs to produce nonwovens, is also known as spunbonding process.^[94] Recently, a mixture of

Table 2. List of techniques, materials, and observed air filtration properties for selected melt-spun and melt-blown air filters.

Product ^{a)}	Filter characteristics f \varnothing = fiber \varnothing [μm]	Pollutant/ size [μm]	Max. removal efficiency [%]	Airflow/velocity [L min ⁻¹]	Pressure drop [Pa]	QF [Pa ⁻¹]	Dominant filter mechanism(s)
PP/ PET composite filter with biocidal agent ^[90]	f \varnothing 0.25–0.8	Paraffin mist 0.4	95	30	180	N/A	Electrostatic capture
		Bioaerosol <i>S. aureus</i> 0.5	99.9				
PS/ PP multi-scale fabric membrane ^[91]	f \varnothing 0.3–8, porosity 87–93%	NaCl 0.26	99.9	32	42	0.18	Electrostatic capture
PP/ PEG micro-nanofiber filter ^[92]	f \varnothing 0.8–1.5	NaCl 0.26	85	0.05 m s ⁻¹	50	0.03	Interception, Brownian diffusion
PLA electret fabric filter ^[93]	f \varnothing 0.1–6.0	Aerosol particles 0.3–0.5	88.5	0.05 m s ⁻¹	41	N/A	Electrostatic capture
TiO ₂ / Ag/ PP on PE/PET nonwoven ^[95]	f \varnothing 4–16	NaCl 0.3	98	85	68–94	0.02	N/A
		<i>E. coli</i> , <i>S. aureus</i>	99.3				
PP/ MgSt air filter ^[96]	f \varnothing 2	NaCl 0.26	99.2	85	92	0.05	Electrostatic capture
PP/PC/ZIF-8 nanofiber membrane ^[97]	N/A	DEHS 0.2–2.5	91.7	57	46	0.05	Diffusion, interception, inertial impaction

^{a)} N/A: not available.

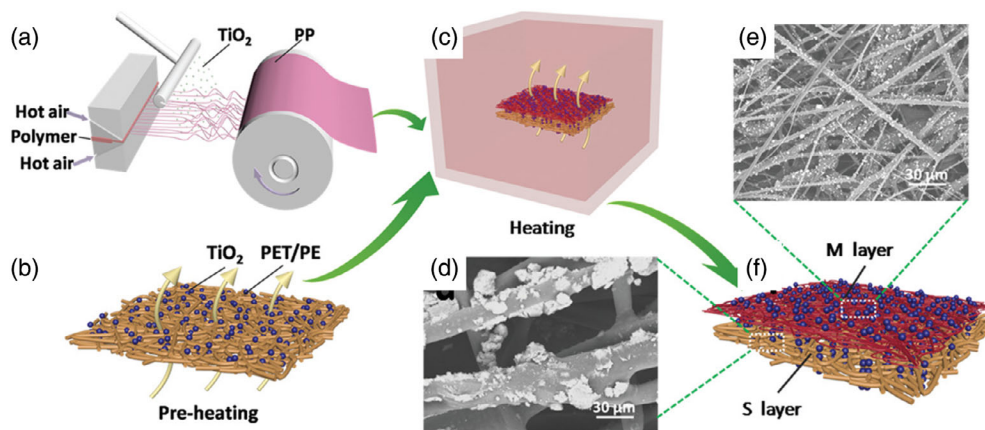


Figure 5. Combination of melt blowing and spun bonding: a) Melt-blown TiO₂/PP nonwovens are combined with b) preheated PE/PET spunbond layers by c) a heating process in a vacuum oven at 140 °C for 1 h under the pressure of 50 N, yielding f) hierarchically structured composite air filters, as shown in SEM images of d) spun-bond layer and e) melt-blown layer. S and M refer to the spun and melt layers, respectively. Reproduced with permission.^[95] Copyright 2019, John Wiley and Sons.

photocatalytically active TiO₂ and antibacterial silver was incorporated into melt-blown polypropylene (PP) fibers. This was achieved by online powder spraying of the particles onto the freshly generated fibers and subsequent thermal conjunction with spunbond layer into a hierarchically structured composite, as shown in **Figure 5**.^[95] The addition of nucleating agents such as magnesium stearate (MgSt) particles to the matrix polymer could enhance the filter charge by improving the crystal structure. Subsequent corona charging, which was carried out by applying high potentials on the material, upon discharge resulted in the deposition of ions in the electret material.^[96] The incorporation of particles during fiber processing usually comes along with possible nonuniform distribution of the particles, low particle loads, and wrapping of the particles with the polymer matrix. An alternative approach is the in situ growth of materials, e.g., high surface area ZIF-8 nanocrystals, on the melt-blown fibers, making more nanocrystals available on the fiber surface.^[97]

The performance of coarse-fibred melt-spun and melt-blown air filters cannot quite keep up with the performance of fine-fibred electrospun air filters with respect to the filtration efficiency. However, efficiencies of more than 85 % were reported for melt-spun and melt-blown air filters, see **Table 2**. Efficiencies higher than 99 % were reported for polymeric PS/poly(ethylene terephthalate) (PET) and PS/PP and composite TiO₂/Ag/PP and PP/MgSt air filters. At the same time, melt-spun and melt-blown air filters yielded consistently low pressure drop values, mostly below 100 Pa. This allows for convenient breathing resistances. The major filter mechanisms for melt-spun and melt-blown air filters were found to be electrostatic capture and interception. Overall, melt spinning and melt blowing enable a satisfactory trade-off between production efforts and production rates on the one hand, and air filtration performance on the other hand.

4.3. Solution Blow Spinning

Solution blow spinning, also called solution blowing, is a method in which a polymer solution is pumped through an inner nozzle,

whereas a constant high-velocity gas flow is provided through an outer nozzle. Solution blow spinning combines the solution-based approach of electrospinning with the conventional blow spinning technique. This allows for a high rate production of nonwoven meshes of micro- and nanofibers without the need for high voltage equipment.^[98] With common fiber diameters slightly lower than 1 μm, see **Table 3**, solution blow spun fibers are equal in size or only slightly wider than electrospun fibers. The most important processing parameters to tailor the properties of the resulting fiber mats are the polymer concentration and gas pressure.^[99] As the deposition rate of solution blow spinning can be ten to thirty times higher than that of conventional electrospinning,^[100] it was expected to become the new vanguard in polymer fiber mesh production. But the predicted success was not achieved yet. However, the method was utilized successfully in the production of cellulose, PAN, PVDF, PMMA, Nylon 6, and other fiber meshes used as air filters.^[101–103] Recently, a multi-needle blow spinning device was presented, which allows for large-scale production of PI air filters.^[104] Thereby, polyamic acid was used as a precursor and transferred into PI nanofibrous membranes by thermal imidization. Other than that, ceramic yttria-stabilized zirconia (YSZ) nanofiber sponges were produced by blow spinning of a polymeric precursor solution containing zirconium *n*-propoxide and yttrium nitrate hexahydrate into a porous cage and subsequent calcination, as shown in **Figure 6**.^[105]

The performance of air filters fabricated by solution blow spinning is characterized by medium to high filtration efficiencies, which can exceed 99%, see **Table 3**. Coarse and fine PMs were retained by polymeric air filters, whereas inorganic YSZ filter could also successfully retain ultrafine PM. At the same time, the pressure drop values remained in the double-digit range. However, the air velocity was very low. Polymeric composite air filters showed similar pressure drop values at considerably high airflows, but also lower efficiencies. Impaction, interception, and diffusion were reported to be the major filter mechanisms for air filters produced by solution blow spinning.

Table 3. List of techniques, materials, and observed air filtration properties for selected solution blow-spun air filters.

Product ^{a)}	Fiber \varnothing [nm]	Pollutant/ size [μm]	Max. removal efficiency [%]	Airflow/ velocity [m s^{-1}]	Pressure drop [Pa]	QF [Pa^{-1}]	Dominant filter mechanism(s)
Cellulose diacetate nanofibers	950	Cigarette smoke 0.3–10	76	1784 L min^{-1}	63	0.02	Inertial impaction, diffusion, interception
PAN nanofibers on PET	590		92		50	0.05	
PVDF nanofibers on PET in commercial nonwoven PP mask ^[101]	660		74		70	0.02	
Nylon 6 mats on nonwoven pp ^[102]	206–356	PS latex particles 0.3	93.5	0.05	30	0.09	N/A
PAN nanofibers on large- scale nylon mesh ^[103]	150–200	Incense smoke 0.3–10	99.9	0.7	380	0.02	N/A
PI nanofibrous membrane ^[104]	380, pore size 5.8 μm	NaCl	99.7	N/A	126	N/A	Inertial impaction, interception, diffusion, electrostatic capture
YSZ nanofiber sponge ^[105]	400	NaCl 0.02–0.6	99.4	0.05	57	N/A	Interception

^{a)}N/A: not available.

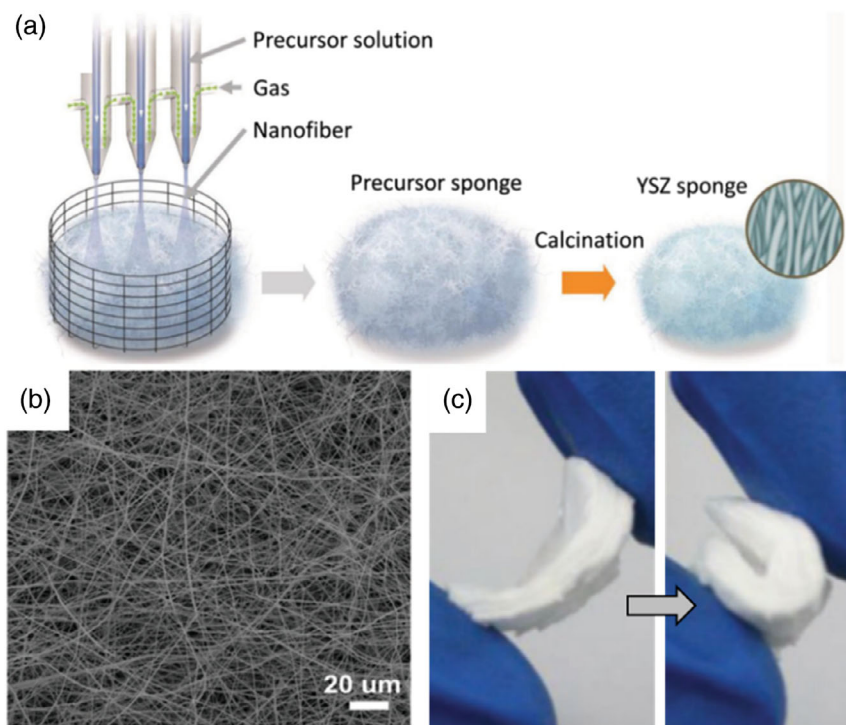


Figure 6. Blow spinning of flexible ceramic YSZ nanofiber sponges: a) The polymeric precursor solution containing zirconium *n*-propoxide and yttrium nitrate hexahydrate is injected from the inner nozzle of a syringe onto a porous cage, whereas airflow is provided at the exit from the outer shaft. b) SEM image shows the formation of c) a homogeneous YSZ nanofiber sponge after heat treatment at 800 °C, which can be repeatedly bent. Adapted with permission.^[105] Copyright 2018, John Wiley and Sons.

4.4. Miscellaneous Spinning Techniques

Apart from the techniques described earlier, there are numerous other spinning techniques available that can be applied to form fibers and fiber meshes. One example is the flash spinning

technique, in which a polymer solution is heated and pressurized in an autoclave assembly before being transported through orifices into a lower pressure zone, yielding 3D nonwoven networks called plexifilaments.^[106,107] Blend spinning and sea/island conjugated spinning are other techniques based on different degrees

of polymer dissolution, where the sea component has a higher dissolution rate than the island polymer. In the former one, the polymer melt blends are spun, whereas for the latter one, the sea and island polymers are melt separately before being extruded into the spinneret, followed by combined spinning.^[108] The following removal of the sea component, generally by dissolution, results in the formation of ultrafine fibers, e.g., made from polyethylene (PE). Centrifugal spinning uses a rotating spinning head, from which the spinning fluid is ejected as soon as the centrifugal force overcomes the surface tension of the spinning fluid.^[109] Hollow fibers and fiber membranes of polyethersulfone (PES), PAN, PVDF, and PAN/PVDF, to be used as air filters, were produced by a dry-jet wet spinning approach.^[110,111] During this process, a polymer solution and bore fluid are fed into the outer and inner tubes of a spinneret. Solidified hollow fiber membranes can be obtained after passing through a water coagulant bath.

4.5. Nonspinning Techniques

As discussed earlier, most spinning techniques can produce fibers and fiber-like structures that can be directly used as air filters. However, there are also traditional methods which can be used to fabricate air filters such as: i) carding of fibers into a continuous yarn, ii) weaving or knitting them to produce meshes or fabrics, and iii) adding the produced soft fabrics to a mechanical support before being used as filter medium.^[112] In this regard, needle punching is used to mechanically interlock preassembled fiber webs, e.g., by integrated preceding fiber lay-down or separately with the help of a carding machine and cross-lapper, using barbed needles.^[113] During needle punching, the barbs on the needles pick up fibers and carry them into the structure, whereby the fibers are entangled and form a coherent nonwoven fabric. Product properties, such as porosity and filter performance, can be predominantly tailored by choice of material, initial web structure, needle penetration depth, and punching density.^[114] The orientation of the fibers and pressure drop was found to decrease with increasing feeder speeds.^[115] In contrast, fiber orientation and filtration efficiency could be increased with increasing the cylinder and doffer speeds. Although the textile industry mostly used it for fabric production, needle punching was also successfully applied for the production of PE, PP, acrylic, as well as recycled PE and cotton-based polymeric air filters.^[116–118] Aramid nonwovens, manufactured by carding and bonding, were recently impregnated in phosphoric acid to generate a large number of nanofibrils on the fiber surface and subsequently impregnated with CuO–CeO₂ catalysts, allowing for easily scalable production.^[119]

Other elaborated methods include freeze drying of nanofiber suspensions, e.g., from MOF-functionalized cellulose.^[120,121] In this regard, ultralight 3D nanofibrous aerogels for energy-efficient filtration of ultrafine airborne particles were recently produced by freeze drying of crosslinked electrospun PAN mats or from pullulan/PVA.^[122,123] The freeze drying method allows obtaining air filters with porosities higher than 99%, see **Table 4**. Nonwoven polymeric substrates can be coated with 2D or 3D structures to tailor the filter architecture and properties. For instance, commercially fabricated nylon cloth was decorated with silver nanowires (NWs) by vacuum filtration as well as by

economic and fast dip-coating process, allowing to fabricate 7.5 m² filter material within 20 min.^[124,125] Dip coating was also applied to cover catalytically treated PET nonwovens with aluminum, whereby the coating time could be adjusted to tailor the resulting surface roughness.^[126] Similarly, aluminum was applied on catalytically treated PE air filters by dip-coating the polymeric filters into an aluminum precursor ink and subsequent heating.^[127] However, this synthesis must be carried out in a moisture-free argon atmosphere. Recently, a novel, combined approach of layer-by-layer assembly, electrophoretic deposition, and dip-coating was used to produce electrostatic air filter on nonwoven fabrics.^[128] Thereby, TiO₂ NPs were deposited on self-assembled layers of poly(diallyl dimethylammonium chloride) and poly(sodium 4-styrenesulfonate) anchored on a PE nonwoven and subsequently dip coated with silver NWs. Moreover, blade coating, during which a blade is used to distribute and simultaneously remove the excess coating, leaving behind a thin layer of coating within the porous substrate, was used to coat a nonwoven substrate with GO.^[129] In addition, a salt solution was coated on PU fiber filters, resulting in the deposition of sea salt particles on the filter surface.^[130] Flexible, fibrous composite fibers were successfully prepared by simple drying of denatured protein with nano- and microcellulose suspensions on a thermal platform.^[131] Recently, an antipathogen nanostructured silica matrix doped with silver nanocluster was coated on glass fiber-based air filters by means of a radio frequency cosputtering process, utilizing two cathodes made from silver and silica.^[132]

Prefabricated, noncontinuous, ceramic short fibers can be shaped into fibrous air filters by different techniques. Vacuum filtration was used to bond ceramic fibers such as polycrystalline mullite fibers through a sol to form fiber node that enhances the matrix strength upon calcination.^[133,134] The final morphology of the fibers, e.g., whiskered, tasseled, or branched, could be tuned by adjusting the mass ratio of active powder and sintering temperature.^[134] Furthermore, stable fibrous ceramic membranes were produced by simple pressing of ceramic mullite fibers with suitable binders, such as abundant kaolin and feldspar, and sacrificial pore-forming agents such as corn starch.^[135,136] These ceramic membranes were used directly as air filters or further modified, e.g., by spray-coating spherical Al₂O₃ to decrease the pore size and to enhance the surface area and roughness.^[135,136] Common pore sizes are in the range of a few hundreds of a millimeter, see **Table 4**.

Short ceramic nanofibers could also be unidirectionally grown in situ on ceramic foams replicated from polymeric foams, e.g., by catalyst-driven conversion of preceramic polymers with additional carbon nanofibers upon pyrolysis, yielding Si₂N₂O NW-decorated SiC foams, as shown in **Figure 7a**.^[137] This type of filter is also called hairy foam due to its resemblance with hairs in the nasal cavities.^[138–140] Other fiber materials such as CNTs were coated on glass fiber substrate by an additive technology called electroaerodynamic jet printing or electroaerodynamic deposition (EAD).^[141,142] In this process, prefabricated CNTs were aerosolized, electrically charged, injected through a nozzle, and deposited on the substrate by application of an electric field at atmospheric pressure and temperature.

Direct growth of fibrous layers of CNTs on different substrates is most widely achieved by chemical vapor deposition (CVD).^[143,144] During the process, a hydrocarbon gas is passed

Table 4. List of techniques, materials, and observed air filtration properties for selected fibrous air filters produced by various other techniques.

Product ^{a)}	Filter characteristics $f\phi = \text{fiber } \phi [\mu\text{m}]$	Pollutant/ size $[\mu\text{m}]$	Max. removal efficiency [%]	Airflow/ velocity $[\text{m s}^{-1}]$	Pressure drop [Pa]	QF $[\text{Pa}^{-1}]$	Dominant filter mechanism(s)
Carded/needle-punched aramid fiber filter with surface nanofibrils and CeO-CeO ₂ catalyst ^[119]	Pore size 19 μm , SSA 12.3 $\text{m}^2 \text{g}^{-1}$	NaCl 0.3	85	32 L min^{-1}	3.5	0.5	Diffusion, interception
PAN aerogel on HEPA H13 filter ^[122]	$f\phi$ 0.2–0.3, porosity > 99%	Incense smoke < 2.5	99.9	0.1	54	0.11	Electrostatic capture
Nanofibrous pullulan/PVA aerogel ^[123]	Porosity 93.9–98.4%	DEHS 0.2	99.998	0.02	550	0.02	Interception
Ag NWs dip coated on large-scale nylon mesh, voltage applied ^[124]	N/A	Sandal-wood smoke (ionized) 2.5	99.7	0.2	14	N/A	Electrostatic capture
Ag NWs vacuum filtrated on nylon, voltage applied ^[125]	$f\phi$ 40 and 0.3	Incense smoke (ionized) 2.5	> 99.99	0.1	3.5	N/A	Electrostatic capture
TiO ₂ NP and Ag NW decorated PE air filter electrodes ^[128]	Interfiber distance 30–120 μm	Incense smoke (ionized) 2.5	99	0.05	11	0.42	Electrostatic capture
Blade coated GO membrane on nonwoven fabric ^[129]	N/A	Sandal-wood smoke 2.5	99.5	0.1	7	0.75	Adsorption
Thermally dried flexible nanoprotein/ cellulose composite filter ^[131]	$f\phi$ 0.05–0.08	Incense smoke 0.3 2.5–5	88 99.9	0.04	92	0.015– 0.075	N/A
Vacuum filtrated SiO ₂ bond mullite fiber composite membrane ^[133]	$f\phi$ 5–10	Incense smoke 0.3	90	0.3	60	0.038	Interception, inertial impaction, diffusion, electrostatic capture
Slurry filtrated hierarchical mullite fiber network ^[134]	Porosity 83–89%, pore size 50 and 1 μm	Particles 0.5 0.3	94 57	28.5 L min^{-1}	N/A	N/A	N/A
Si ₂ N ₂ O ₂ NWs grown on SiC foam ^[137]	$f\phi$ 0.2–0.4, porosity 85%	NaCl 0.08–0.3	99.997	0.08	237	N/A	Interception, diffusion
Electro-aerodynamic deposited CNTs on glass fiber filter ^[141]	$f\phi$ 0.05	Bio-aerosol Bacteriophage MS2, <i>E. coli</i> 0.04	92 78.4	0.2	80	0.02	Adsorption + puncture and damage of microbes by CNTs
Pressed mullite fibrous ceramic membrane ^[135]	Pore size 25–60 μm , main pore size 47 μm	Dust 0.3	82	0.02	80	N/A	N/A
Spray-coated Al ₂ O ₃ on mullite fibrous ceramic membrane ^[136]	Pore size 20–50 μm , main pore size ca. 30 μm	Dust 0.3	91.6	0.03	280	N/A	N/A
Salt spray coated PU fiber filter ^[130]	$f\phi$ 1–8, salt particles 0.1 and 0.9 μm	Bio-aerosol <i>E. coli</i> , <i>S. epidermidis</i> 0.8	98.5	0.07	186	N/A	N/A + lethal change of osmotic pressure

^{a)}N/A: not available.

through a reactor containing metallic NPs to catalyze the hydrocarbon decomposition at elevated temperatures, yielding CNTs with a variety of diameters ranging from 1 nm to 10 μm , see **Table 5**. CNTs were deposited on glass fiber meshes^[141,145–147] and inorganic porous foam structures.^[148–152] Furthermore, CNTs could be deposited on stainless steel as a substrate material, which upon the attack of supersaturated carbon vapor, generated in situ by the decomposition of a solid organic precursor, acts as a catalyst source to initiate the CNT growth, as shown in Figure 7b.^[153] Most commonly, the catalyst is loaded ex situ prior

to the CVD process using an aerosol, allowing a nonuniform coating of the catalyst due to a disturbed air flow by nearby fibers. Thus, CNTs are exponentially decreased along the filter thickness, allowing to achieve a CNT gradient within the filter structure.^[145] It is also possible to process free-standing CNT filters on low-adhesion materials, from which they can be easily transferred by dry-press transfer to any substrate.^[154] In addition, subsequent functionalization by acid treatment followed by a polyol process could be applied to deposit metal NPs, e.g., silver NPs, on the surface of on CNTs.^[148]

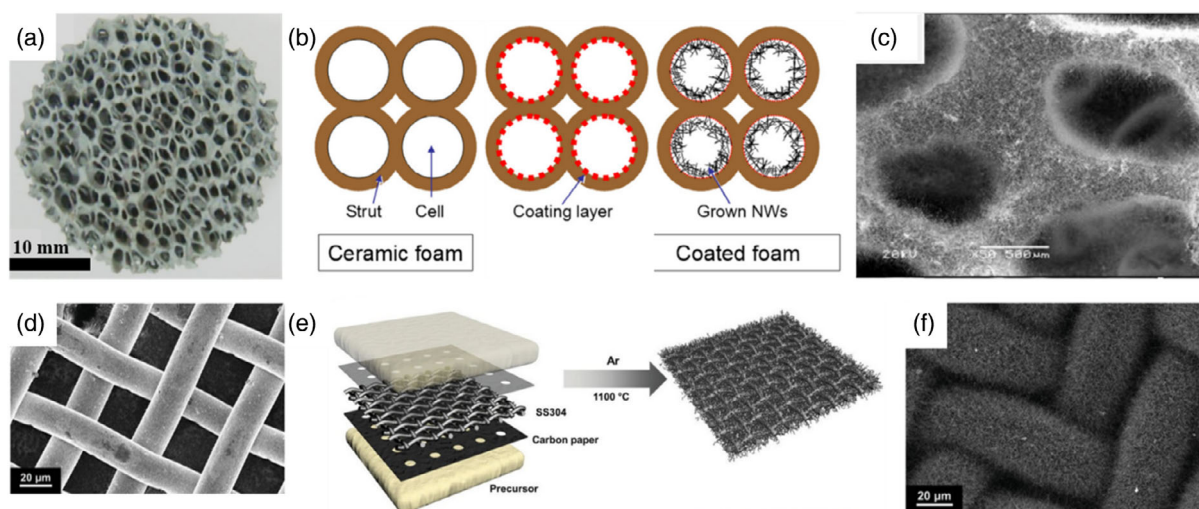


Figure 7. NW growth on inorganic substrates. Top: unidirectional growth of $\text{Si}_2\text{N}_2\text{O}$ NWs on SiC foam: Photograph of a) 40 ppi SiC foam, b) schematic of the process, c) SEM image of NW coated SiC foam. Adapted with permission.^[137] Copyright 2015, Elsevier. Bottom: in situ vapor growth method of carbon NWs by decomposition of solid organic precursor on stainless steel substrate, which serves as catalyst source: d) SEM image of the stainless steel substrate, e) schematic of the method, and f) SEM image of the substrate with carbon NWs. Adapted with permission.^[153] Copyright 2019, John Wiley and Sons.

Table 5. List of techniques, materials, and observed air filtration properties for selected fibrous air filters produced by CVD.

Product ^{a)}	Filter characteristics $f\phi = \text{fiber } \phi$ [nm]	Pollutant/ size [μm]	Max. removal efficiency [%]	Airflow/ velocity [m s^{-1}]	Pressure drop [Pa]	QF [Pa^{-1}]	Dominant filter mechanism(s)
Hierarchical CNT quartz fiber filter ^[145]	$f\phi$ 10–30	DEHS	99.99	0.05	435	0.02	Inertial impaction, diffusion
Ag@MWCNTs nano-network on Al_2O_3 substrate ^[148]	Pore size 2.8 μm , porosity 44%	SiO_2 0.3 Bioaerosol <i>E. coli</i> , <i>B. subtilis</i> , <i>A. niger</i>	99.9999 100	0.02	4650	0.003	N/A
CNTs on AC fiber substrate ^[152]	$f\phi$ 8000–10000	NaCl 0.02–0.3	96	0.06	30	0.1	N/A
Carbon NWs on stainless steel substrate ^[153]	$f\phi$ 120	Incense smoke 2.5	96.7	0.1	258	N/A	N/A
Free-standing SWCNT film ^[154]	$f\phi$ 1.3–2	Fe 0.01	99.99	0.3 L min^{-1}	229	0.06	N/A

^{a)}N/A: not available.

With only a few exceptions, air filters produced by nonspinning techniques show filtration efficiencies over 99%, see Table 4 and 5. The highest efficiencies and lowest pressure drops, i.e., the highest QFs, were achieved by composite, multiscale fibrous structures decorated with NWs as well as by fabrics blade coated with GO. The dominant filter mechanisms for the former and the latter air filters were reported to be electrostatic capture and adsorption, respectively. The extraordinary electrostatic capture was induced by the external inducement of electrostatic interactions, i.e., by applying a voltage on the air filter, and ionizing the pollutant. In contrast, the pressure drop is commonly higher for intrinsically charged

air filters. However, those air filters do not require a power supply and thus, are also suitable for nonstationary applications. Bioaerosols containing bacteria and viruses were filtered and destroyed by fibrous air filters containing CNTs and sea salt. Fibrous air filters produced by CVD showed superior removal efficiencies, but also higher pressure drops of mostly a few hundred Pa, see Table 5, which are higher than those reported for air filters fabricated by other nonspinning techniques. However, most of the composite and inorganic fibrous air filters provided promising air filtration performances when considering their mainly straightforward, economic processing, and optimization routes.

5. Processing Technologies and Performance of Nonfibrous Air Filters

Processing methods to obtain i) open cellular solids, made up of interconnected networks of solid struts or plates forming cell edges, and ii) granular air filters, including granules or grains as deployed in fixed or fluidized bed filters as well as structures made from granules and grains, will be discussed in the following sections.

5.1. Cellular Air Filters

Different types of foams and porous structures could be prepared by several techniques, including direct blowing, phase separation, replica, etching, thermal decomposition, etc.^[155–166] Recently, single-layer polyimide (PI) film air filters were patterned with thru-holes by ion milling, which allows fabricating micrometer holes of defined sizes by photolithography.^[167] More common than thin, single-layer filters are thicker filters, often accompanied by larger pore sizes. Commercially produced, economic, and permeable PU foams were used as air filters as well as bactericidal coatings.^[168,169] The coating was obtained by immersing the filter structure into quaternized PU solution and subsequent drying. Prefabricated melamine foams were successfully coated with bio-based ionic polymers derived from alginate and used as air filters.^[170] Furthermore, air filters were also obtained by direct blowing. A typical blowing process for the production of cellular PI/zeolite foams is shown in **Figure 8**. Thereby, isocyanate reacts with water to produce CO₂ and primary amines that create pores in the foam during the release of CO₂ within the mixture of PI precursor and zeolite.^[171] The blowing process allows for the direct incorporation of large amounts of copper and nickel micrometer-sized particles into the PI foams.^[172] In the course of this, it is important to accurately adjust the amount of water and solvent to prevent the open cell porous structure from collapsing. Recently, nanoporous carbon foams, fabricated via NaCl-assisted pyrolysis from edible feedstocks, were coated onto nonwoven fabrics by traditional dip coating.^[173]

Aerogels, which can be produced by supercritical, freeze, or ambient pressure drying of gels, are believed to have a promising future in air filtration due to their high porosity, surface area, and adjustable surface chemistry.^[174–177] For example, combining a classical sol–gel process with freeze drying allows for the synthesis of plant-based composite aerogel air filters from konjac fibers and wheat straw.^[178] Similarly, nanocellulose aerogels as high-performance air filters were fabricated by freeze drying of 2,2,6,6-tetramethylpiperidine-1-oxyl-oxidized cellulose nanofibril dispersions in water/*tert*-butyl alcohol mixtures.^[179] Furthermore, cellulose aerogel made from waste cotton was carbonized in argon atmosphere and molybdenum disulfide nano-sheets were hydrothermally grown on the surface.^[180] Aerogel air filters based on modern polymers, such as polystyrene (PS) and PI, were fabricated by supercritical drying of their corresponding gels.^[181,182] In addition, inorganic graphene aerogel air filters were produced by freeze drying of GO hydrogel and subsequent solvent exchange with water to carry out conventional freeze drying.^[183] Inorganic hydroxyapatite (HAP) aerogel air filters were obtained by freeze drying aqueous slurries containing hydrothermally produced HAP.^[184] Treatment of the hydrophilic HAP aerogel in ethanol removed the surface oleate layer, rendering it hydrophobic.

Ion-mediated assembly (IMA) is another approach used for the production of carbon-based aerogels.^[185,186] During IMA, a porous network of nanoplatelets, most commonly from GO, is produced by soaking a conductive mesh and plate made from conductive copper or nichrome, respectively, into a vessel containing the respective suspension.^[185] Upon application of a constant voltage and resulting electrostatic force, the nanoplatelets adhere to the surface. Subsequent freeze drying transfers the hydrogels into aerogels. Furthermore, a heat treatment is commonly followed to transform the GO into reduced GO (rGO) to enhance conductivity. Aerogels generally have high porosities and can strongly differ in their pore size, see **Table 6**.

Additive manufacturing (AM) was also followed for the production of air filters, whereas less common, as they are rather unsuited for large-scale production. For dust filtration, biomimetic villus-structured acrylonitrile butadiene styrene (ABS)

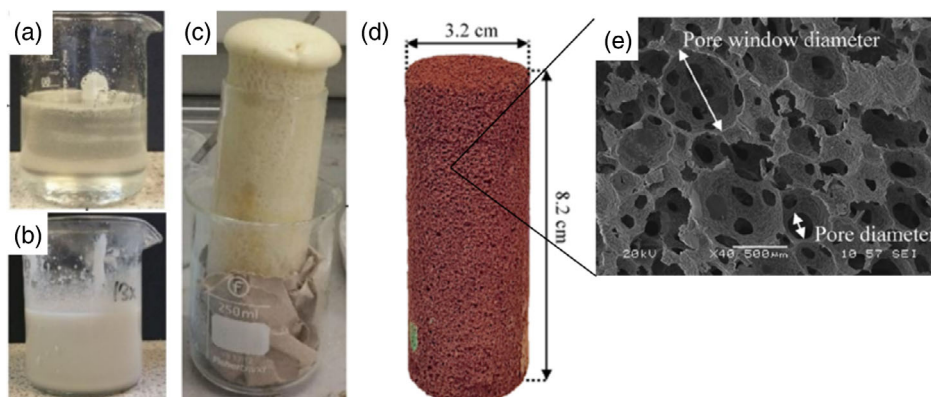


Figure 8. Open cell-structured foams by simultaneous blowing and polymerization reaction. Left: photographs of the reaction of PI/zeolite foam showing a) the precursor mixture containing pyromellitic dianhydride (PMDA), 1-methyl-2-pyrrolidone (NMP), amine catalyst, and silicon oil, b) the addition of zeolite powder and tin catalyst, and c) the foaming process upon the addition of isocyanate. Adapted with permission.^[171] Copyright 2019, Elsevier. Right: d) Photograph and e) SEM image of a PI/Cu composite foam. Adapted with permission.^[172] Copyright 2020, American Chemical Society.

Table 6. List of techniques, materials, and observed air filtration properties for cellular air filters.

Product ^{a)}	Filter characteristics	Pollutant/ size [μm]	Max. removal efficiency [%]	Airflow/ velocity [m s ⁻¹]	Pressure drop [Pa]	QF [Pa ⁻¹]	Dominant filter mechanism(s)
PU foam ^[168]	Foam rib thickness 37–54 μm, porosity 50–90 ppi	Fungal spores	73.5	N/A	N/A	N/A	N/A
Alginate-based ionic polymer on melamine foam ^[170]	Rib thickness 5–10 μm	PM 2.5 10 <i>E. coli</i>	99.7 99.9 92.7	0.5	2	2.29	Electrostatic capture + cell membrane damage
PI/Cu/Ni foam ^[172]	Porosity 74–82%, pore size 71–296 μm	Bacterial aerosol	99.9997	1 L min ⁻¹	N/A	N/A	N/A
Flexible thin-film lift off GO/PANI filter ^[28]	Pore size 3.2 nm	Incense smoke 2.5	99.7	N/A	8270	N/A	Sieving
Free-standing laser-induced graphene foam filter on PI lattice ^[29]	Pore size 2.9–8.4 nm	Cigarette smoke 0.01–0.6	>86	10 L min ⁻¹	250	N/A	Sieving
Nanoporous carbon foam on nonwoven ^[173]	N/A	Cigarette smoke 2.5	99.4	0.25	112	N/A	N/A
PI aerogel ^[182]	Porosity 91–98%	NaCl 0.025–0.15	99.999	20 L min ⁻¹	840	N/A	N/A
Charged graphene aerogel filter, voltage applied ^[183]	SSA 13 m ² g ⁻¹	Incense and cigarette smoke (ionized) 0.3–10	99.9	0.72	0.5	14	Electrostatic capture
HAP aerogel filter ^[184]	Porosity 99.7%	Incense smoke 2.5–10	99	0.025	167	N/A	Adsorption, interception
MoS ₂ nanosheet decorated carbonized cellulose aerogel, voltage applied ^[180]	SSA 378 m ² g ⁻¹	Incense smoke (ionized) 2.5 10	99.9 99.95	0.3	0	N/A	Electrostatic capture
Freeze-casted lignin/GO based aerogel filter ^[195]	Pore channel size 20–40 μm	Incense smoke 0.1	99.75	0.05	90	0.07	Diffusion
Freeze-casted Si ₃ N ₄ filter ^[196]	Pore size 0.3–50 μm, porosity 63–70%	Fly ash 4.4	99.99	3.8 L min ⁻¹	1400	N/A	N/A
Charged rGO hydrogel on copper mesh, voltage applied ^[185]	Pore size several tens of microns	Incense smoke (ionized) 2.5	>99.9	0.2	5	1.8	Electrostatic capture
rGO aerogel on nichrome mesh, voltage applied ^[186]	Pore size 7.3 μm	Dust, FPM, CPM (ionized) 2.5	99.9	2.5	7	N/A	Electrostatic capture
Vacuum filtrated waste paper hollow air filter ^[197]	SSA 118 m ² g ⁻¹ , holes of 0.5–2 cm	Incense smoke 2.5	99.2	5	34	N/A	Adsorption

^{a)}N/A: not available.

filters were recently prepared by vat polymerization.^[187] These filters exhibit surface areas three times higher compared to those of planar structured filters. More recently, flexible 3D air filters from g-C₃N₄ photocatalyst and poly(ethylene glycol) diacrylate (PEGDA) polymer were printed using the robocasting technique followed by freeze drying.^[188] Furthermore, 3D printed PU was used to mechanically stabilize electrospun PAN nanofiber mats.^[189]

Among other techniques, freeze casting is a powerful and environmentally friendly method that was applied to produce air filters. Freeze casting allows producing aligned pores in

the casted materials by sublimation of ice formed during unidirectional freezing of slurry.^[190–194] Lignin-based air filters with uniformly aligned, micrometer-sized pores were obtained by freezing alkali lignin solutions mixed with GO sheets, freeze drying, and subsequent annealing at 300 °C to induce crosslinking.^[195] Similarly, controlling the freezing and sintering temperatures also allowed tailoring the pore size and microstructure of Si₃N₄-based air filters,^[196] see Table 6. Thin-film lift-off, during which a polymer or composite of polyaniline (PANI) and GO is dissolved and cast on a glass plate, followed by solvent evaporation, yielded flexible composite filters.^[28] Recently, direct

laser writing was explored for the production of air filters. Thereby, direct photothermal conversion of a carbon precursor such as PI film was achieved by CO₂ laser cutting, during which noncarbon elements are outgassed, and sp² hybridization of the carbon species is promoted, yielding microporous conductive graphene foams.^[29] Furthermore, air filters made from oxidized waste paper were produced by basic vacuum filtration.^[197] After thermal oxidation in aqueous solution, the waste paper solution was vacuum filtrated into molds and compressed, yielding an interconnected spider web structure made of cellulose. Therein, one or several holes were drilled to evoke turbulent flow.

The performance of cellular air filters is characterized by filtration efficiencies as high as 99% and above, as shown in Table 6. At the same time, the pressure drop fluctuates more strongly in comparison with fibrous air filters. Several cellular air filters, mostly based on carbon-based aerogel structures, reached pressure drops as low as 0–0.5 Pa using electrostatic capture, enhanced by the application of a voltage. Accordingly, they achieved very high QFs. However, other cellular air filters, e.g., made from polymeric composites and waste paper, were also able to successfully filter coarse PM at a pressure drop of only 34 Pa by means of intrinsic electrostatic capture and adsorption, respectively, for air velocities as high as 5 m s⁻¹. In contrast, very high pressure drops in the range of a several hundreds of Pa were observed for polymeric PI aerogels, composite GO/PANI filters, or inorganic Si₃N₄ filters, already at low air flows. The reason behind is the utilization of very small pore sizes for size-based filtration by sieving on the one hand. On the other hand, for larger pores, it can be presumed that the obtained structure does not provide sufficient tortuosity to allow for sufficient air flow. Overall, cellular air filters were shown to be able to compete with fibrous air filters in terms of air filtration performance. At the same time, cellular air filters allow to be processed by a wider variety of processing techniques, coming along with a considerable number of possibilities to tailor the properties and resulting performance.

5.2. Granular Air Filters

AC is one of the most common granular air filter materials, usually deployed in bed filters. It can basically be synthesized from any carbon-based material by thermal, chemical, or steam pyrolysis, during which carbonization and activation, often with KOH or NaOH as activating agents, yields high porosity and high surface area granules with mostly micro- and mesopores.^[14] Within the broad range of possible precursor materials, natural materials such as olive stones did attract attention and were successfully activated by physical CO₂ activation.^[198] Granular bed filters made from nanosilver/TiO₂-chitosan composite could be produced by crosslinking colloidal suspensions of chitosan and TiO₂.^[199] During this process, beads were shaped using a peristaltic pump, and subsequently covered with silver NPs by photochemical deposition.

Uniaxial or hydrostatic pressing and subsequent sintering of ceramic powders, such as SiC, Al₂O₃, MgO, or low-cost ceramic materials with sacrificial pore-forming agents, e.g., fugitive organic materials, is a simple and common processing technique to obtain granular ceramic materials that can be used as air filters.^[200–202] Metallic air filters, e.g., made from nickel, were also fabricated by uniaxial pressing.^[203] Air filters produced by pressing commonly have pore sizes within a few micrometers and porosities up to 70%, see Table 7. Spray coating of SiC with oxide mixtures and methyl cellulose as a pore-forming agent onto pre-fabricated substrates were utilized to obtain porous mullite, ZrSiO₄, and CaSiO₃-bonded SiC membranes.^[204] However, it is important to prevent penetration of the spray-coated filter layer into the support. This can be achieved by means of insertion of a whisker-based interlayer, as shown in Figure 9. Furthermore, dip coating was utilized for the generation of active layers on substrates such as La-TiO₂ on ceramic membranes.^[205]

The performance of granular air filters is not yet capable of competing with fibrous and cellular air filters. Although all inorganic granular air filters listed could achieve remarkable removal

Table 7. List of techniques, materials, and observed air filtration properties for selected granular air filters.

Product ^{a)}	Filter characteristics	Pollutant/ size [μm]	Max. removal efficiency [%]	Airflow/ velocity [m s ⁻¹]	Pressure drop [Pa]	QF [Pa ⁻¹]	Dominant filter mechanism(s)
Mullite bonded porous SiC ^[200]	Pore size 2–18 μm, porosity 29–56%	NaCl 0.007–0.3	99.9	0.05	5700–15000	0.001	N/A
Cordierite bonded porous SiC ^[201]	Pore size 6–50 μm, porosity 30–72%	NaCl 0.007–0.3	99.99	0.05–0.1	1144	N/A	Diffusion
Nickel filter ^[203]	Pore size 1–2 μm	NaCl 0.02–0.45	99.9	2.3 mol s ⁻¹ m ⁻²	10000	N/A	Diffusion
AgNPs@ TiO ₂ -chitosan hydrogel beads bed filter ^[199]	Sphere Ø 1.5–2 mm	Bacterial and fungal bioaerosol 1.0–1.56	98	1.5 L min ⁻¹	40	0.1	Interception + cell membrane damage
Spray-coated SiC on SiC support ^[204]	Pore size 2.3 μm	Aluminum 0.3	99.95	0.03	1190	N/A	N/A

^{a)} N/A: not available.

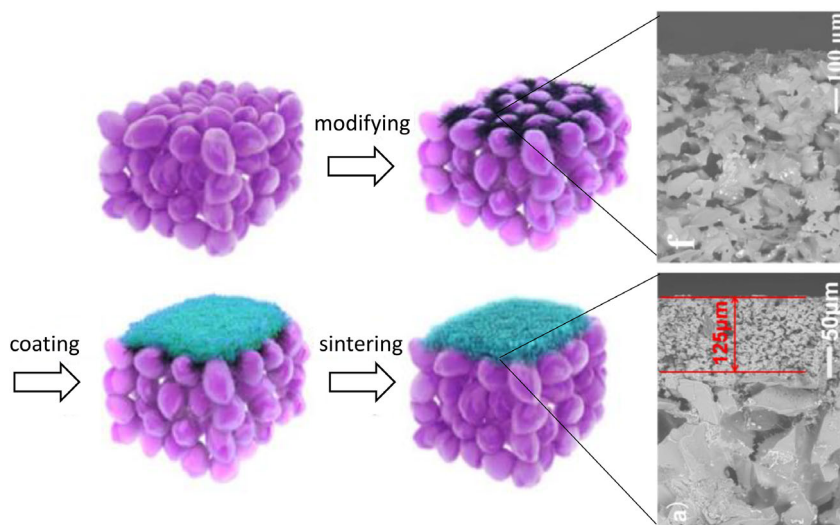


Figure 9. Schematic of the spray-coating process of SiC: The original SiC support (purple) is modified with SiC whiskers (black) by spray coating the respective suspension to prevent penetration of the subsequently spray-coated SiC powder (green). Adapted with permission.^[204] Copyright 2017, Elsevier.

efficiencies higher than 99.9%, their high pressure drop values, i.e., in the range of several hundreds to thousands of Pa, at comparably low air velocities diminish their performance, see Table 7. However, granular air filters have the potential to be further optimized to reach better performances. First steps into that direction were recently taken with the development of a hydrogel composite beads filter, able to successfully filter bacterial and fungal bioaerosols by interception instead of diffusion. Nevertheless, the challenge remains to achieve moderate pressure drops for practicable air velocities and airflows.

The major air filter performance criteria, i.e., removal efficiency, pressure drop, as well as the QF, serving as a benefit-to-cost ratio, are graphically shown in **Figure 10** for the fibrous, cellular, and granular air filters made from polymeric, composite, and inorganic materials discussed in this Review. In addition to the removal efficiency and pressure drop, the air velocity was considered, as the pressure drop commonly increases with increasing air velocity for air filters utilizing conventional filter mechanisms, as discussed. Hence, the greater part of the fibrous air filters exhibits high removal efficiencies at pressure drops mostly below 300 Pa, which was considered as maximum breathing resistance for FFP3 masks. However, the majority of fibrous filters were tested at comparably low air velocities. In contrast, for cellular air filters in particular, electrostatic pollutant capture using external voltages was shown to achieve high removal efficiencies at high air velocities while maintaining low pressure drop values. Similar results could be obtained by polymeric, cellular air filters utilizing the adsorption mechanism, as described earlier. Overall, cellular air filters recently became increasingly competitive with fibrous air filters, which can also be observed from the QF. Although cellular air filters are reported in a relatively small number of works in comparison with fibrous filters, they show the highest QFs, i.e., $\geq 1.8 \text{ Pa}^{-1}$, see Figure 10. As the QF is inversely proportional to pressure drop, see Equation (4), outstanding QFs can only be achieved for filters with low

pressure drops. As shown in Figure 10, high QFs of $0.5\text{--}1 \text{ Pa}^{-1}$ can be found for several fibrous air filters, produced by modern electrospinning processes as well as blade coating and traditional carding and needle punching processes, with pressure drops lower than 10 Pa. However, the majority of the fibrous air filters exhibit QFs of $0.02\text{--}2 \text{ Pa}^{-1}$ with pressure drops of $50\text{--}200 \text{ Pa}$, which is sufficient for most application areas. For granular air filters, there is not yet enough data for a meaningful comparison. However, granular air filters tend to show higher pressure drops for similar filtration efficiencies in relation to

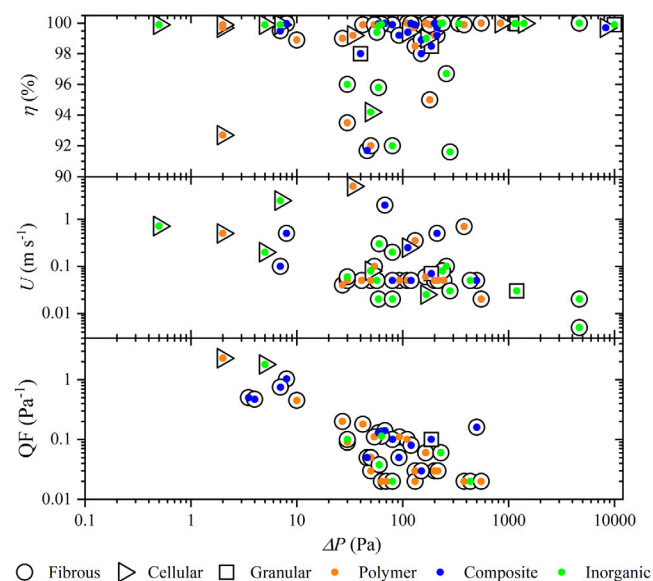


Figure 10. Graphical representation of the pressure drop ΔP versus removal efficiency η , air velocity U , and QF, respectively, for the fibrous, cellular, and granular air filters made from polymeric, composite, and inorganic materials, as shown in Table 1–7.

fibrous and cellular air filters. With regard to the material class, no material was found to be clearly superior as an air filter material. However, a clustering of PU.^[48,77] and GO-based^[70,129,185] materials can be found among the air filters with the highest QFs. Both, polymeric and inorganic materials provide different properties, which can be specifically tailored. The formation of composites allows tailoring of both the structural and material's properties in order to increase the filtration efficiency and restrict pressure drop, i.e., increase the QF, as will be described in the following sections.

6. Tools for Air Filter Performance Enhancement

In the following, an overview of the influence of structural and materials properties on the air filter properties and techniques will be provided. In addition, tools to equip filter materials with antimicrobial properties, as well as the capability to filter gaseous pollutants, will be given. Finally, the regeneration of air filters for multiple uses, in contrast to disposable filters, will be discussed in the framework of sustainability.

6.1. Structural Optimization

Different structural properties, including fiber size, porosity, tortuosity, surface area, and mechanical strength, can strongly influence the properties and application areas of air filters. In general, a reduction of the thickness of the active filtering layer, also called basis weight, is advisable to decrease the pressure drop.^[196] To achieve high filter efficiencies, high surface area and roughness are commonly required to enhance pollutant capture.^[74,152] This can be achieved by i) oxygen treatment, e.g., yielding AC with high specific surface areas (SSAs), and ii) shaping materials into geometries that allow for high surface-area-to-volume ratios such as fibrous or pleated structures.

For fibrous air filters, it can be observed that the smaller the fiber diameter, the higher the effective surface area and filtration efficiencies. Thus, it is common to decrease the fiber diameter in the air filters by reducing the polymer concentration, adjusting the solvent system, or incorporating specific inorganic NPs during fabrication to alter the solution's viscosity.^[46,49,57,66,69] When fibers are deposited on substrates, the majority of the fibers is deposited on the grid, and only a few fibers extend into the gaps of the grid. This leaves back areas, which are not covered by the fibers and thus, decrease the filter efficiency. Homogeneous fiber distributions could be achieved by some particular techniques, such as bipolar electrospinning, where the collector is placed

in between the needles.^[63] Coating of nonwoven fiber structures with 2D or 3D materials, such as GO or nanoporous carbon foams, was also used to decrease interfiber voids.^[173] Although for fibrous air filters, a very narrow distribution of fiber diameter results in more compact and efficient fabrics, it also increases the airflow resistance.^[93] Accordingly, optimization of the fiber packing density by i) combining ultrafine high surface area fibers with porous micrometer- and submicrometer-sized beads along the fiber axis to increase the interfiber voids, porosity, and adsorption area,^[49,50,70] or ii) combining micro- with nanoscale fibers,^[65,91,92,134] are frequently used strategies to fabricate air filters with low pressure drop and high efficiencies. The underlying mechanism utilized is called slip flow effect and describes the phenomenon of molecules and particles passing by a fiber without colliding with it and thus, decreasing air resistance. In general, slip flow occurs for small nanofibers. Thus, optimization of the fiber diameter and aperture size of fiber assembly toward the mean free path length of air molecules yielded ultralow pressure drop values while preserving high filtration efficiency.^[206] As shown in **Figure 11**, the slip flow effect could be further enhanced in the olive-like bead structure of GO/PAN air filter. In this structure, GO beads collect the particles from the air, increase the interfiber distance and therewith decrease the likelihood of particles colliding with the fibers, resulting in a lower pressure drop, while preserving high filtration efficiencies.^[70] In addition, the velocity of the pollutant containing gas stream is reduced, and accordingly, the time spent in the filtration medium is prolonged.^[77] As a consequence, the likelihood of capture mechanisms is increased. Furthermore, the beads result in enhanced nanofiber curvature and improvement of the volume fraction by preventing nanofiber bundling, which would decrease the effective filter area.^[207,208] Natural spider webs, in which viscid silk is covered with regularly spaced viscid beads, are used to adhere insects to the surface, utilize the same slip flow effect, too. They were used as model structures for modern nanofiber constructed membranes for solid pollutant interception.^[80]

For cellular air filters, sufficient tortuosity and interconnectivity between the pores need to be ensured to enhance airflow and reduce pressure loss. This was achieved by deliberate generation of microcracks, emerging into nearly straight channels, and unidirectional alignment of the pores as obtained by freeze casting or directional heating.^[133,196,209]

For granular bed filters, small-sized granular mediums have better filtration efficiency than large-sized granular mediums due to the higher surface area, but as already observed for fibrous and

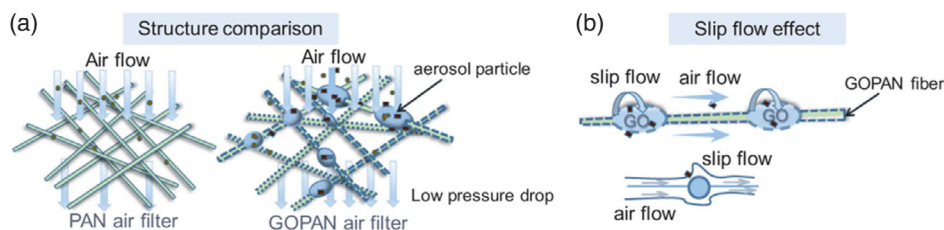


Figure 11. Performance enhancement by bead-on-string structured air filters using the slip flow effect: a) Structure comparison between PAN fiber and PAN fibers with beads made from GO and b) visualization of particle-fiber interaction during slip flow. Reproduced with permission.^[70] Copyright 2018, Elsevier.

cellular structures, this usually does not compensate for the increase in pressure drop.^[210] Therefore, the optimal size of the granular medium strongly depends on the size of the target particles. Dual-layer granular beds, cascading a layer of fine granules on a layer of coarse granules, aid to achieve both high filter efficiencies and low pressure drops.^[211] Hierarchical structures on cellular and granular-based air filters are also commonly achieved by etching, coating, and fiber growth on the surface. This significantly increases filtration performance, but only cause a minor increase in pressure drop. For example, the incorporation of silver particles on multi-walled CNTs (MWCNTs) on Al₂O₃ substrate increased the SSA by a factor of 126 and reduced the average pore size. The produced samples showed the slip effect, which resulted from the silver particles on the MWCNTs, improving the overall filtration performance.^[148]

The orientation of filters with hierarchical structures has a substantial influence on the filtration performance. When the filters are adequately aligned within air flow direction, a gradient of morphologies helps to extend the filter lifetime by removing larger particles prior to smaller ones.^[29] Moreover, clogging of the filter is reduced, which is exemplarily shown in **Figure 12** for fibrous CNTs on quartz filters. When the CNT-rich side is placed upstream, high efficiencies can be achieved initially, followed by rapid clogging, reducing the service life. On the contrary, when the CNT-rich side is placed downstream, the substrate reduces the accumulation of particles on the filter surface, slows down clogging, and reduces the pressure drop rise.^[145] When passing air through hollow filters, the air flow can become turbulent, which increases the possibility for interactions between the pollutants and the air filter.^[197] Single modules of hollow filters with different parameters such as size and number of the inner diameter and the module length can be connected in series to further enhance the removal efficiency and restrict the pressure drop.

It is also possible to coat both sides of the filter with an active layer, yielding a bidirectional nature of the filter capable of simultaneous inside-out and outside-in filtration.^[185] In addition to the

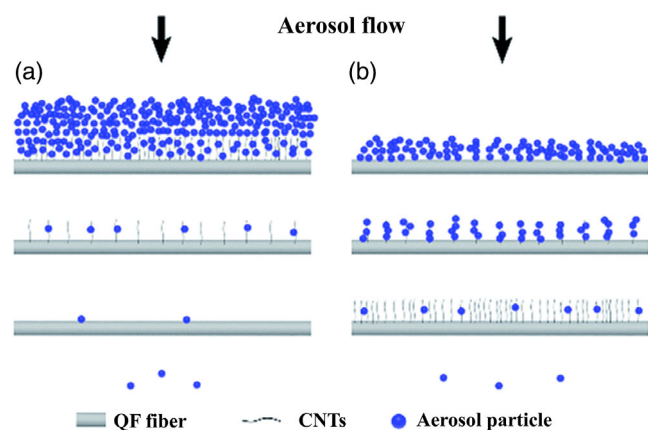


Figure 12. Influence of filter orientation in the airstream on service life schematically represented by gradient CNTs on quartz fiber filter: a) CNT-rich side placed upstream resulting in high efficiency, but rapid clogging, whereas b) placing the CNT-rich side downstream slows down the clogging process. Adapted with permission.^[145] Copyright 2014, The Royal Society of Chemistry.

orientation of the filter within the air flow, the structural assembly of the filter itself has an influence on the air filter properties, especially on its mechanical properties. For instance, the flexibility of YSZ nanofiber sponge filter could be increased with decreasing diameter of the nanofiber and grain size.^[105] A flexible and porous, yet rigid and strong composite structure of graphene reinforced with alternating hexagonal PI lattices was developed. Such structure resembles the stable AB-stacked bilayer graphene and preserves continuity for electrical conductivity.^[29] Holes up to 1 mm could be healed within 5 min due to deposition of CNTs at the edges, maintaining both structural integrity as well as filtration performance.^[154] This can be attributed to the unique properties of CNTs, which exhibit an elastic response for small deformations and a viscoelastic response for larger deformations.

Mechanical properties should be considered, especially for nonstationary air filters, where vibration, shocks, and deformation could potentially lead to defects in the filter and, thus, decreased filter performance. Although there exist numerous flexible air filter materials,^[28,29,81–83,105,124,131,167,188] their highly porous structure makes air filters mechanically less robust than their dense counterparts. Therefore, they are usually deployed on mechanically more robust substrates or reinforced with rigid structures. In general, the mechanical properties of nanofibrous structures depend on the geometric arrangement of fibers, mechanical properties of the fibers, and other components, interactions between fibers, and strength of interfiber bonds.^[67] Thermal imidization of the precursor structure into PI yielded an increase in tensile strength from 2.9 to 8.8 MPa.^[104] The incorporation of 4 wt% silica NPs into PVA–PAA fibers could increase the tensile strength from 5.2 to 6.4 MPa.^[37] CNTs could improve the tensile strength of hybrid filters by 45% in comparison with pure PI nanofiber membranes, yielding up to 9 MPa.^[72] Tensile strengths up to 11.3 MPa could directly be achieved for electrospun PVDF nanofiber/net membranes.^[47] Furthermore, inorganic platinum/Al₂O₃ fibrous membranes with tensile strengths up to 44 MPa could be obtained depending on the platinum concentration and calcination temperature.^[82] The strength could be increased with increasing platinum concentration and decreasing calcination temperature due to the smaller particle size of platinum, and accordingly, a higher amount of grain boundaries formed at lower calcination temperatures. Compressive strength was shown to be increased by lamellar structures of cellulose nanofibers within cellulose-based network.^[120] The resulting hydrogen bonds and physical entanglement yielded an increase in compressive strength by a factor of three up to 485 kPa.

6.2. Material Optimization

Apart from the structural optimization, the selection and optional modification of the materials used for the production of air filters is the second major factor in tailoring the resulting air filter properties. It allows to select and modify materials with regard to their surface properties such as surface charge and extent of hydrophilicity, resistance to elevated temperatures, and harsh chemical environments, as well as optical properties.

Utilizing and tailoring the surface charge of materials became a powerful tool during the development and improvement of modern air filters. Materials with high dipole moments such as the polymers PAN, PVDF, or PBI exhibit better removal efficiencies for particles due to enhanced electrostatic forces with the pollutants.^[47,51,212] In addition, materials from natural resources such as oxidized waste paper exhibit high dipole moments.^[197] However, the surface charge can also be altered for materials with lower dipole moments to generate electrostatic charges within the materials, improving the electrostatic attraction of particles without increasing the pressure drop.

Numerous in situ and postprocessing techniques for charging fibers and fabrics were reported. For instance, in situ charging of PVDF fibers during electrospinning could induce a crystal phase transition from α -PVDF to β -PVDF, resulting in an increase in dipole moment from 5.6 to 9.1 D.^[47] Corona charging was applied on PS/PP and PLA, improving their crystallinity and yielding longstanding charge-trapping properties, resulting in improvements in filtration efficiency of up to 49% compared with their noncharged equivalents.^[91,93] Similarly, tribocharging, utilizing the triboelectric effect from rubbing fibers with dissimilar electronegativity against each other, was shown to yield enhanced filtration properties for PP/modacrylics and PTFE/nylon composite filters.^[213,214]

Electrical charging and tribocharging can also be carried out consecutively, as successfully demonstrated for poly(vinylidene fluoride-co-trifluoroethylene) (PVDF-TrFE) copolymers.^[53] Furthermore, charge enhancers, such as MgSt or HAP, were introduced to enhance the crystallinity and electret performance. Depending on the concentration of MgSt, degrees of crystallinity of up to 46% could be achieved.^[96] The combination of PVDF with HAP in nanowool felts resulted in surface potentials as high as 13,260 V.^[60] Moreover, the incorporation of materials with high dielectric constants such as BaTiO₃ or magnetic Fe₃O₄ improves the charge storage and results in good electret performance.^[64,68] Furthermore, the defects of MOFs such as ZIF-8 could polarize the surface of pollutants, which will then interact with the positively charged ZIF-8.^[80,97] The incorporation of inorganic particle mixtures into polymers with strong surface potentials such as PVDF was found to support the release of negative ions, which effectively capture PM.^[69]

Conductive materials, such as graphene, rGO, and MoS₂ decorated carbonized aerogels could be charged directly by applying a voltage on the filter.^[180,183,185] Voltages were also applied on copper-plated PAN filters, which were found to significantly increase the collection efficiency of charged PM with increasing voltage.^[84,85] Similarly, good filtration efficiencies were achieved with silver NW decorated nylon sheets and aluminum-decorated PET nonwovens.^[124–126] A 3D conducting network made from silver NWs on functionalized PE nonwovens allowed to directly use the air filters as electrodes.^[128] Long-range adsorption of pollutants onto the surface of TiO₂/carbon nanofiber could also be achieved by photoinduced interfacial space-charge polarizations at Schottky junctions, significantly enhancing filtration efficiency for particles smaller than 1 μm .^[83] Incorporation of materials with inherently large amounts of functional groups, such as GO or soy protein isolate, containing abundant hydroxyl, carboxyl, methyl, and amino groups, is another strategy to enhance pollutant capture via electrostatic attraction and adsorption.^[56,70]

In general, utilizing electrostatic attraction as a dominant capture mechanism reduces the problem of increasing pressure drop due to the increase in the amount of captured pollutants as in interception-based filters.

The choice of hydrophilic, hydrophobic, or a combination of hydrophilic–hydrophobic materials allows preserving or improving filtration performance even at elevated levels of humidity. High humidity values can occur at the air filter location or outside of respiratory masks such as in specific world regions or by industrial processes. Furthermore, humidity accumulates on the inside of respiratory masks due to exhaled, moist air. Particle droplets can easily deposit and condense on hydrophilic polymers such as PAN at high humidity values, forming a water film that blocks air flow, as shown in **Figure 13a**, and thus, causes an unwanted increase in pressure drop. With time, water molecules can diffuse through the membrane, see **Figure 13d**. In contrast, hydrophobic materials such as polytetrafluoroethylene (PTFE), PMMA, PVDF, or Al₂O₃ are able to initially repel particle droplets, resulting in a slower increase in the pressure drop,^[54,148,214,215] as shown in **Figure 13c**. With time, the droplets coalesce on the surface and form a continuous liquid film as they cannot be transported across the membrane, compare **Figure 13f**, resulting in an increased pressure drop. When combining an outer hydrophobic layer with an inner hydrophilic layer, particle droplets can be repelled initially, but transmitted through the inner layer, as shown in **Figure 13b,e**, resulting in an overall reduced pressure drop at all times.^[111] This pull–push effect allows for excellent directional moisture transport performance and vapor transmission rate of up to more than 10 kg m⁻² d⁻¹, allowing to preserve the thermal–physiological comfort and the filter performance.^[74]

When considering the material's resistance toward elevated temperatures and harsh chemical environments, not only the application conditions, but also conditions evoked by possible regeneration methods should be considered. An overview of different regeneration methods is provided within the filter regeneration section. In general, resistance toward high temperatures is low for polymers because of their low glass transition temperature. Similarly, polymers have a comparably low resistance to harsh chemical environments. However, these properties allow for the processing of polymer materials at moderate temperatures. Both temperature and chemical resistance can be improved with additives and fillers, yielding composite structures. Resistance toward high temperatures and harsh chemical conditions is usually high for inorganic materials such as ceramics and metals. However, this usually comes along with higher energy needs during the production of inorganic air filters.

Polymeric air filters, in particular, can be tuned according to their optical properties, allowing to yield air filters with high light transmittance. Different materials and compositions such as PMMA/PDMS/chitosan, PU, PAN, and PVDF-TrFE, optionally with TiO₂ NPs or silver NWs, were shaped into (semi) transparent air filters.^[48,53,54,65,103,124,125]

6.3. Antimicrobial Features

If desired, air filters can be equipped with antimicrobial properties, utilizing specific material and structural properties. Because

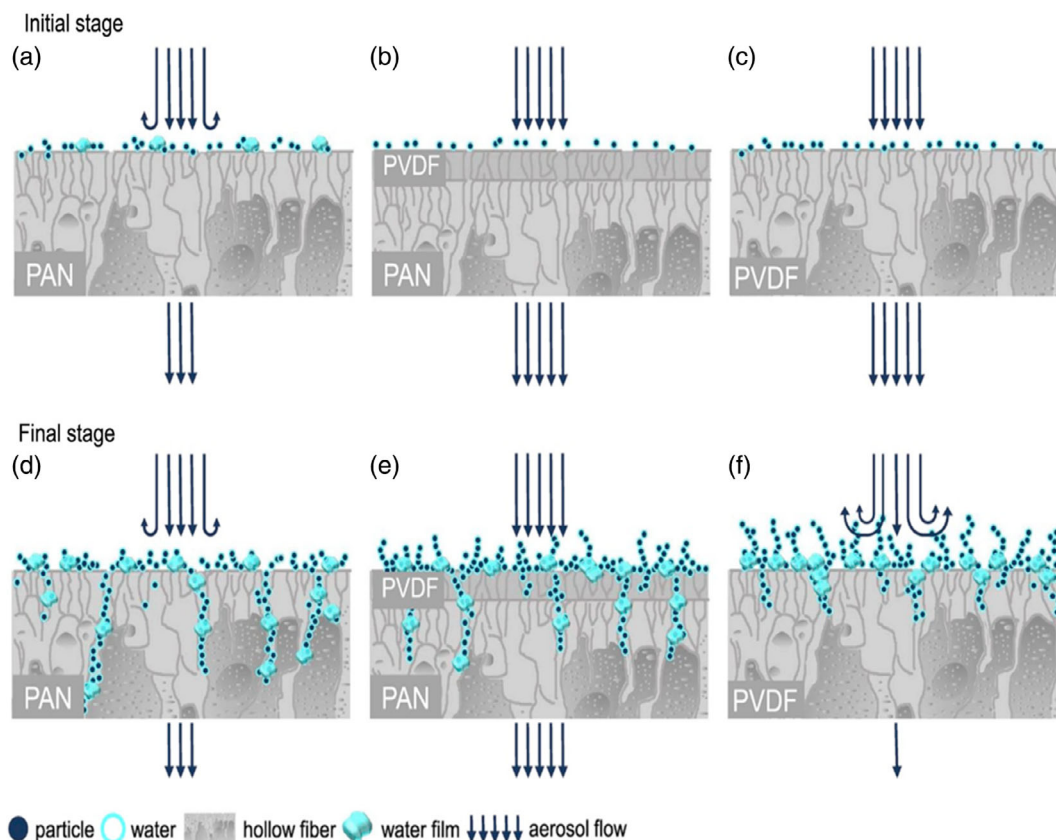


Figure 13. Effect of a,d) hydrophilic materials such as PAN, c,d) hydrophobic materials such as PVDF, and b,e) hierarchical combination of hydrophilic and hydrophobic materials on aerosol deposition and flow. Reproduced with permission.^[111] Copyright 2020, Elsevier.

polar polymers are prone to be contaminated with microorganisms due to their hydrophilicity and organic nature, they should be modified or substituted to eliminate microorganisms.^[81] Long and rod-shaped bacteria *Erwinia carotovora* could grow well on the PI foam filter, as shown in Figure 14a.^[172] Polymers such as polyionic liquids can kill bacteria by destroying their phospholipid bilayer membrane, yielding strong antibacterial properties.^[57] In general, the incorporation of metallic NPs, such as silver, copper, and nickel is a common strategy to achieve antimicrobial properties. These NPs can electrostatically interact with microorganisms, provide high surface areas for cell contact and release metal ions, during which they can disrupt cellular respiration, penetrate the cell membrane, and disrupt metabolic processes.^[76,172,199] The resulting leached and dead bacteria after contacting PI/copper foam filter are shown in Figure 14b. Even when incorporated into a polymer matrix or MOFs, metal ions and organic ligands can be released from metal NPs and MOF crystals.^[67] The incorporation of silver NPs into a silica matrix was even shown to result in a more progressive release of ions, resulting in a long-lasting antipathogenic effect.^[132] Similarly, materials with a positive charge, such as chitosan with its amide groups, were found to interact with cell surfaces of opposite charge and disrupt cell membranes, causing protein leakage and death.^[54,199] Furthermore, salts were utilized as antimicrobial agents, as they induce a shift in osmotic pressure, yielding to lethal damage of microbes.^[130]

Bacteria and viruses can also be successfully damaged mechanically, most commonly by carbon nanostructures. CNTs are able to penetrate cell membranes and inactivate microbes, whereas shorter and single-walled CNTs were shown to be more efficient than longer and multi-walled CNTs outside of liquid systems.^[141,148,216] The mechanical capture and damage of the virus Bacteriophage MS2 by a CNT air filter is shown Figure 14c.^[141] Similar to CNTs, graphene can also mechanically damage microbes due to cutting and entering cell membranes, encapsulating them, inhibiting growth, and generating oxidative stress from the functional groups, resulting in deadly intoxication of the cells.^[29,216]

Irradiation with UV light is a common method for air filter disinfection of microbes, both during filtration and for regeneration. However, the comparably low penetration depth of UV irradiation limits its efficacy. UVA and UVC radiation are not suitable for thorough disinfection, as byproducts of the microorganism death are not destroyed upon irradiation. Biological endotoxins are left behind. On the contrary, treatment with UVD irradiation was found to transform bound endotoxins in *E. coli* bioaerosols into free endotoxins and subsequently degrade them due to the generation of ozone, as schematically shown in Figure 14d.^[217] Thereby, bound endotoxins are transformed into free endotoxins and subsequently degraded. However, ozone itself is an air pollutant. Its generation can be avoided using photocatalytic materials such as MOFs, which reliably kill airborne

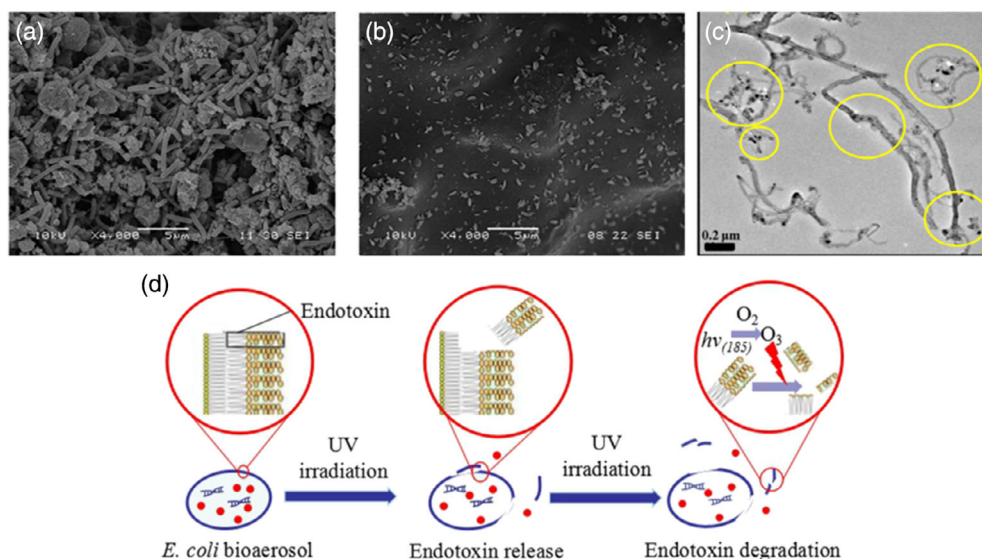


Figure 14. a) Live, well-grown bacteria on a PI foam filter and b) dead, flat and grain-like bacteria on a PI foam filter incorporated with 80 wt% Cu. Reproduced with permission.^[172] Copyright 2014, Elsevier. c) TEM image of the mechanical capture and damage of viruses by CNT air filter. Adapted with permission.^[141] Copyright 2020, American Chemical Society. d) Schematic description of the degradation mechanism of endotoxins by UVD irradiation through ozone degradation. Reproduced with permission.^[217] Copyright 2019, Elsevier.

bacteria within 30 min by the production of reactive oxygen species upon UV irradiation.^[218] Similarly, UV irradiation of TiO₂ NWs was found to generate high levels of reactive oxygen species, while exhibiting enhanced wettability for germ-carrying droplets.^[219]

6.4. Filtration of Gaseous Pollutants

Proper choice of material and processing allows equipping particulate air filters with additional filtration abilities for gaseous pollutants, if required. Pollutants are captured by structures with high SSAs and high amounts of functional surface groups. Afterward, hazardous pollutants can optionally be converted into non- or less hazardous substances, most commonly by UV or visible-light-assisted photocatalytic oxidation.

Gelatin and soy protein composites were found to be successful in the adsorption of formaldehyde with removal efficiencies of up to 91%.^[55,56,71] The amine groups of the biopolymers can bond with the aldehyde group of the formaldehyde, forming aldime linkages. Air filters from waste paper could maintain formaldehyde removal efficiencies over 71% due to their abundant oxidized groups.^[197] Moreover, ZIF-8@SiO₂ composite membranes exhibit chemical adsorption capacities for formaldehyde of up to 146 mg g⁻¹ due to the large cavities, abundant gas adsorption sites, and functional groups of the ZIF-8 nanocrystals.^[80] For an initial formaldehyde concentration of 2.45 mg m⁻³, the removal efficiency reached up to 79.5%. ZIF-69/PS nanofiber membranes were found to achieve physical adsorption capacities of up to 1362 mg g⁻¹ for SO₂.^[75] AC, known for its capability to remove ozone from the air by reactions with surface oxide groups, was found to preserve removal efficiencies of more than 99% even upon surface growth of CNTs.^[152] Furthermore, AC, with its high surface area, large number of active functional moieties, and its

tendency to intercalate VOCs within its interface layers, is capable of adsorbing 51% of toluene with an initial concentration of 4.5 ppm.^[77] In addition, VOCs could be removed by functionalization of nonwovens with β-cyclodextrin without affecting the air permeability.^[220]

Incorporation of the well-known TiO₂ photocatalyst into silver and PP composite air filter could achieve an effective degradation of 93.4% of toluene under irradiation with UV light.^[95] In the process, degradation is ensured by oxidation of the pollutant by free hydroxyl radicals on the TiO₂ surface. Similarly, Ag@CNTs composite with a high surface area was applied to effectively catalyze the oxidation and degradation of formaldehyde under UV light.^[148] Thereby, the CNTs provide a high SSA for pollutant capture and vacancy deficiencies, which result in a surface oxygen activation of the silver NPs, yielding degradation rates of more than 80 % and 99.99 % at room temperature and 55 °C, respectively. Researchers today are increasingly focusing on photocatalytic materials whose bandgaps allow for the utilization of visible solar lights. In that regard, photocatalytic degradation of nitrogen oxide over the surface of C₃N₄ in a polymeric matrix could be achieved by irradiation with visible light.^[188] Furthermore, the doping of TiO₂ with recycled lanthanum was shown to increase nitrogen oxide degradation under visible light by 33% compared with pure TiO₂, yielding a removal efficiency of 98%.^[205] Furthermore, CuO–CeO₂ catalysts on air filters were shown to effectively photodegrade toluene and CO upon xenon lamp irradiation.^[119]

6.5. Filter Regeneration

With regard to increasing worldwide awareness of sustainability, efforts are made to produce air filters, which can be regenerated by cleaning in liquid or via heat treatment without compromising

their mechanical stability and filtration efficiency. Air filters should be replaced or regenerated when their filter efficiency or pressure drop falls below or exceeds a specific value, respectively, depending on the application. For instance, HEPA filters are commonly replaced when the pressure drop reaches two times the initial value.^[221]

Especially for materials with low thermal stability, such as polymer-based air filters, liquid cleaning is a promising way for regeneration over several filtration-wash-dry cycles. Solvents like water with or without detergents, diluted acid mixtures, ethylene glycol, and ethanol, optionally assisted with sonication, were successfully used to remove PM and nitrates, allowing for stable filtration over various filtration cycles.^[51,54,97,124,125,128,167,188,214] Inorganic materials benefit from liquid cleaning methods, too. Adsorbed dust can be easily removed from materials such as rGO, carbonized aerogel, and cellulose by simple soaking due to the polarity of water, enabling up to 270 filtration and regeneration cycles without significant performance loss.^[180,185,186,197] Similarly, ethanol was used to effectively clean graphene aerogel filters, resulting in a slight decrease in its efficiency after multiple cycles and short regeneration times.^[183] Air filters coated with aluminum were found to be easily regenerable by soaking in water.^[126,127]

Heat treatment is suitable for materials with sufficient thermal stability of at least 250 °C or more for safe sterilization of objects via dry heating to remove endotoxins.^[222] This allows polymers such as PI to be thermally regenerated.^[104] Usually, even higher temperatures of more than 500 °C are applied to remove adsorbed PM by calcination of inorganic air filters, such as Ag@SiO₂-TiO₂ or Pt/Al₂O₃, over several cycles without visible efficiency attenuation.^[81,82] Inactivation of SARS-CoV-2 could already be achieved at 85 °C on commercial N95 respirators.^[223] About 50 heat treatment cycles could be carried out without significant change in the filtration efficiency, allowing for safe reuse in times of global shortage of respirators. Conductive air filters, such as carbon NWs on stainless steel substrates or graphene foam, could be renewed via decomposing PM by Joule-induced heating, i.e., by passing a current through the filter to produce thermal energy.^[29,153] In addition, graphene can directly trap contaminants and decrease the resistivity due to its negative thermal coefficient of expansion.^[29] Catalytic air filters, which adsorbed gaseous substances like toluene, can be reactivated multiple times by vacuum drying at significantly lower temperatures of 80 °C.^[95] Regeneration from antimicrobial residues can also be carried out by means of UV irradiation of the used filters, as described in the previous section.

7. Conclusions

In this Review, the fundamental principles of air filters and the evaluation of their performance were elucidated. An overview of the classification and worldwide standardization of air filters was provided. NaCl and DEHS are recommended as nonoily and oily model pollutants because of their suitable shape and ability to form stable aerosols, respectively.

Various processing production routes of fibrous and nonfibrous air filters, considering the influence of processing parameters on the air filter structure, were summarized. For fibrous air

filters, electrospinning allows to precisely control the resulting fiber diameters and shapes using mixed solvent systems or the incorporation of NPs, among others. By today, electrospinning comes in a variety of modifications, which result in more homogeneous fiber meshes. It was successfully applied to produce polymeric, composite, ceramic, and metallized air filter structures. Due to the electrospinning triumph, other techniques such as melt spinning, melt blowing, or solution blow spinning were less intensively explored in the recent past. However, they offer valuable advantages, including high production rates and waiving of high voltage equipment. To widen the image, the possibilities of techniques less common for the production of fibrous air filters, such as freeze drying, dip coating, or CVD were presented. They are suitable for the production of inorganic air filters, in particular. Furthermore, the processing variety of nonfibrous, i.e., cellular and granular, air filters, was presented. Among them, the production of polymeric and inorganic aerogels as air filters is currently gaining importance. However, techniques such as freeze casting, AM, or pressing allow for custom pore size tailoring and hierarchical structures.

The tailoring of several structural parameters and their influence on the air filter properties was discussed. Air filter performance can be improved by increasing the surface area and roughness to enhance pollutant capture as well as utilization of hierarchical structures and considering their orientation along the air flow to reduce clogging. For fibrous air filters, lower fiber diameters come along with higher filter efficiencies. However, optimization of fiber packing by combining micro- with nanoscale fibers and porous beads along the fiber axis allows minimizing airflow resistance and thus, improving overall performance. For nonfibrous air filters, sufficient tortuosity needs to be ensured. Structural optimization was found to be more progressed for fibrous air filters, resulting in overall higher filter performances compared with nonfibrous air filters. However, nonfibrous high-performance air filters were also presented, which in part can already compete with the prevalent fibrous air filters.

The importance of material selection was also presented. Utilizing the material's surface charge became a powerful tool in developing modern air filters, which commonly rely on electrostatic capture mechanisms to decrease the pressure drop. However, specific polymers and ceramics have high dipole moments and dielectric constants on their own, others can be charged in situ or ex situ. Conductive materials allow for voltage application during the filtration process, which is practicable for stationary air filters, in particular. Portable air filters as used for respiratory masks require other solutions and face other obstacles such as accumulating humidity inside the mask due to exhaled, moist air. The smart combination of hydrophilic with hydrophobic materials allows achieving moisture transport that preserves both comfort and performance.

Furthermore, tailoring structural and material properties allows for customizing the antimicrobial properties, rendering viruses and bacteria harmless, most commonly by the release of metal ions or mechanical damage. Additional gas filtration and degradation capabilities can be used by materials with functional surface groups aiding in adsorption and incorporation of photocatalytically active materials. The possibility for air filter regeneration mainly depends on the material's resistance toward

chemicals and high temperatures. Hence, some polymers, but mainly inorganic materials, can be easily regenerated by liquid cleaning or heat treatment, contributing to garbage avoidance.

8. Future Perspectives

Worldwide increasing awareness for sustainability needs to reflect in the production and usage of modern high-performance air filters. Following green chemistry principles,^[224] harmful materials and solvents should be replaced with more environmentally friendly ones. This affects solvent-based spinning techniques in particular and makes other processing techniques worth further exploration. To extend the service life of air filters, reusable air filters, in contrast to disposable air filters, should become the default option. Therefore, material's development and regeneration methods need to be improved and geared to each other. Cheap and available regeneration methods, such as microwave heating or infrared radiation, can be exploited in this process. Ceramic air filters, currently applied for high-temperature applications, may be suitable for room temperature applications, too, or could be tailored accordingly. The utilization of machine learning algorithms provides another promising level of air filter optimization, both during production and operation.^[225] The utilization of alternative energy sources for the operation of electrically charged air filters, e.g., by incorporating radial piston triboelectric nanogenerators,^[226] is expected to gain more importance.

Equipping filters with sensors and/or thermochromatic materials to detect gas or particle concentrations and the body temperature is another future perspective that could help monitor the pollutant concentration and detect sickness of fevering people. In enhancing the antimicrobial properties of air filters, metal oxide NPs should be considered as promising, more economical alternatives for common noble metal NPs.^[227] Furthermore, the wearing comfort of face masks and respiratory masks needs improvement. Novel geometries and skin-friendly materials, preventing painful pressure marks on the skin during long-time usage, should be considered in addition to the filter performance. The utilization of skincare products on the inside of masks could further reduce strain to the skin. Hearing impaired and dumb people would substantially benefit from transparent, filtering masks, allowing for both communication and protection.

However, quick detection of air filters with the best performance, among other custom requirements, remains a challenge due to varying test procedures and incomplete data to some extent. The establishment of common test procedures or application of available standards, already during the research phase, would improve comparability. Furthermore, the important parameter pressure drop could be more easily accounted for if provided by exploiting its predominantly linear dependence on the air velocity. Therefore, researchers could directly provide the linear regression slope (Pa s m^{-1}) instead of only single data points, where applicable.^[228] Looking ahead, air filters may also be tested in other atmospheres, researching their suitability for extraterrestrial applications, e.g., on planet mars.

The transformation of research findings into large-scale production processes is necessary to provide high performance air filters in sufficient quantity. Mass production is also

accompanied by cost reduction, making air filters more easily available. In polluted cities, translucent, air filtering facades could protect the people inside from harmful outdoor pollutants.^[229] During local outbursts or pandemics, AM provides the possibility for near-time and decentral production of air filters and mask housings.

Acknowledgements

A.A. expresses his gratitude to the German Academic Exchange Service (DAAD) for their scholarship support (grant number 91611173). C.V.A. acknowledges the support of the Alexander von Humboldt (AvH) Foundation.

Conflict of Interest

The authors declare no conflict of interest.

Keywords

air filters, cellular polymers, fibrous polymers, granular polymers, processing techniques

Received: January 5, 2021

Revised: February 19, 2021

Published online: March 26, 2021

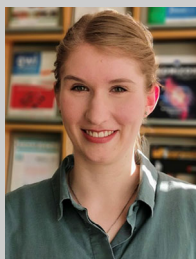
- [1] World Health Organization, *WHO Global Conference on Air Pollution*, World Health Organization, Geneva, Switzerland **2018**.
- [2] UN environment programme, *Air pollution and climate change: two sides of the same coin* **2019**.
- [3] B. E. Howard, *Otolaryngol. Head Neck Surg.* **2020**, *163*, 98.
- [4] C. D. Zangmeister, J. G. Radney, E. P. Vicenzi, J. L. Weaver, *ACS Nano* **2020**, *14*, 9188.
- [5] L. P. Haslett, *Inhaler or Lung Protector US Patent No. 6529*, **1849**.
- [6] G. Liu, M. Xiao, X. Zhang, C. Gal, X. Chen, L. Liu, S. Pan, J. Wu, L. Tang, D. Clements-Croome, *Sustainable Cities Soc.* **2017**, *32*, 375.
- [7] H. Liu, C. Cao, J. Huang, Z. Chen, G. Chen, Y. Lai, *Nanoscale* **2020**, *12*, 437.
- [8] K. O'Dowd, K. M. Nair, P. Forouzandeh, S. Mathew, J. Grant, R. Moran, J. Bartlett, J. Bird, S. C. Pillai, *Materials* **2020**, *13*, 3363.
- [9] M. H. Chua, W. Cheng, S. S. Goh, J. Kong, B. Li, J. Y. C. Lim, L. Mao, S. Wang, K. Xue, L. Yang, E. Ye, K. Zhang, W. C. D. Cheong, B. H. Tan, Z. Li, B. H. Tan, X. J. Loh, *Research* **2020**, 7286735.
- [10] B. Robert, G. Nallathambi, *Colloid Interface Sci. Commun.* **2020**, *37*, 100275.
- [11] Y. Li, X. Yin, J. Yu, B. Ding, *Compos. Commun.* **2019**, *15*, 6.
- [12] V. V. Kadam, L. Wang, R. Padhye, *J. Ind. Text.* **2018**, *47*, 2253.
- [13] H. Souzandeh, Y. Wang, A. N. Netravali, W.-H. Zhong, *Polym. Rev.* **2019**, *59*, 651.
- [14] P. P. Bhave, D. Yeeswarapu, in *Global Challenges in Energy and Environment*, Springer, Singapore **2020**, p. 65.
- [15] P. Li, C. Wang, Y. Zhang, F. Wei, *Small* **2014**, *10*, 4543.
- [16] J. A. Bernstein, N. Alexis, C. Barnes, I. L. Bernstein, A. Nel, D. Peden, D. Diaz-Sanchez, S. M. Tarlo, P. B. Williams, *J. Allergy Clin. Immunol.* **2004**, *114*, 1116.
- [17] A. K. Pahari, B. S. Chaulan, *Engineering Chemistry*, Laxmi Publication, Bangalore, India **2006**.
- [18] Y. Feng, Y. Li, L. Cui, *Fuel* **2018**, *224*, 801.

- [19] A. A. Almetwally, M. Bin-Jumah, A. A. Allam, *Environ. Sci. Pollut. Res. Int.* **2020**, *27*, 24815.
- [20] F. Zhu, R. Ding, R. Lei, H. Cheng, J. Liu, C. Shen, C. Zhang, Y. Xu, C. Xiao, X. Li, J. Zhang, J. Cao, *Respir. Med.* **2019**, *146*, 57.
- [21] R. D. Brook, *Clin. Sci.* **2008**, *115*, 175.
- [22] R. Dhand, J. Li, *Am. J. Respir. Crit. Care Med.* **2020**, *5*, 651.
- [23] I. Manisalidis, E. Stavropoulou, A. Stavropoulos, E. Bezirtzoglou, *Front. Public Health* **2020**, *8*, 14.
- [24] C. Hong, Q. Zhang, Y. Zhang, S. J. Davis, D. Tong, Y. Zheng, Z. Liu, D. Guan, K. He, H. J. Schellnhuber, *PNAS* **2019**, *116*, 17193.
- [25] C. G. Nolte, T. L. Spero, J. H. Bowden, M. S. Mallard, P. D. Dolwick, *Atmos. Chem. Phys.* **2018**, *18*, 15471.
- [26] I. M. Hutten, *Handbook of Nonwoven Filter Media*, Butterworth Heinemann, Amsterdam **2016**.
- [27] K. Darcovich, K. A. Jonasson, C. E. Capes, *Adv. Powder Technol.* **1997**, *8*, 179.
- [28] C. Park, A. S. Johnston, H. Kweon, *J. Appl. Polym. Sci.* **2020**, *38*, 49149.
- [29] M. G. Stanford, J. T. Li, Y. Chen, E. A. McHugh, A. Liopo, H. Xiao, J. M. Tour, *ACS Nano* **2019**, *13*, 11912.
- [30] H. Bensalah, S. A. Younssi, M. Ouammou, A. Gurlo, M. F. Bekheet, *J. Environ. Chem. Eng.* **2020**, *8*, 103807.
- [31] L. M. Henning, U. Simon, A. Gurlo, G. J. Smales, M. F. Bekheet, *RSC Adv.* **2019**, *9*, 36271.
- [32] A. A. Nada, M. F. Bekheet, S. Roualdes, A. Gurlo, A. Ayral, *J. Mol. Liq.* **2019**, *274*, 505.
- [33] A. Buekens, N. N. Zyaykina, L. Xianwei, *Adsorption of Gaseous Pollutants*, EOLSS, Oxford **2009**.
- [34] L. Boskovic, I. E. Agranovski, I. S. Altman, R. D. Braddock, *J. Aerosol. Sci.* **2008**, *39*, 635.
- [35] T.-C. Lin, G. Krishnaswamy, D. S. Chi, *Clin. Mol. Allergy* **2008**, *6*, 3.
- [36] C. Liu, P.-C. Hsu, H.-W. Lee, M. Ye, G. Zheng, N. Liu, W. Li, Y. Cui, *Nat. Commun.* **2015**, *6*, 6205.
- [37] M. Zhu, D. Hua, H. Pan, F. Wang, B. Manshian, S. J. Soenen, R. Xiong, C. Huang, *J. Colloid Interface Sci.* **2018**, *511*, 411.
- [38] C. Pei, Q. Ou, D. Y. Pui, *Sep. Purif. Technol.* **2021**, *255*, 117679.
- [39] E. P. Fischer, M. C. Fischer, D. Grass, I. Henrion, W. S. Warren, E. Westman, *Sci. Adv.* **2020**, *6*, eabd3083.
- [40] D. H. Park, Y. H. Joe, A. Piri, S. An, J. Hwang, *J. Hazard. Mater.* **2020**, *396*, 122640.
- [41] Z. Zeng, R. Grigg, *Transp. Porous Med.* **2006**, *63*, 57.
- [42] D. Lasseux, F. J. Valdés-Parada, *Comptes Rendus Mécanique* **2017**, *345*, 660.
- [43] H. Ma, D. W. Ruth, *Transp. Porous Med.* **1993**, *13*, 139.
- [44] W. E. Teo, S. Ramakrishna, *Nanotechnology* **2006**, *17*, R89.
- [45] N. Vinh, H.-M. Kim, *Appl. Sci.* **2016**, *6*, 235.
- [46] M. Cao, F. Gu, C. Rao, J. Fu, P. Zhao, *Sci. Total Environ.* **2019**, *666*, 1011.
- [47] H. Liu, S. Zhang, L. Liu, J. Yu, B. Ding, *Adv. Funct. Mater.* **2020**, *30*, 1909554.
- [48] R. Chen, X. Zhang, P. Wang, K. Xie, J. Jian, Y. Zhang, J. Zhang, Y. Yuan, P. Na, M. Yi, J. Xu, *Nanotechnology* **2019**, *30*, 15703.
- [49] Z. Wang, C. Zhao, Z. Pan, *J. Colloid Interface Sci.* **2015**, *441*, 121.
- [50] J. J. Huang, Y. Tian, R. Wang, M. Tian, Y. Liao, *Sep. Purif. Technol.* **2020**, *237*, 116377.
- [51] S. Lee, A. R. Cho, D. Park, J. K. Kim, K. S. Han, I.-J. Yoon, M. H. Lee, J. Nah, *ACS Appl. Mater. Interfaces* **2019**, *11*, 2750.
- [52] H. Liu, S. Zhang, L. Liu, J. Yu, B. Ding, *Adv. Funct. Mater.* **2019**, *29*, 1904108.
- [53] K. S. Han, S. Lee, M. Kim, P. Park, M. H. Lee, J. Nah, *Adv. Funct. Mater.* **2019**, *29*, 1903633.
- [54] H. Liu, J. Huang, J. Mao, Z. Chen, G. Chen, Y. Lai, *iScience* **2019**, *19*, 214.
- [55] H. Souzandeh, Y. Wang, W.-H. Zhong, *RSC Adv.* **2016**, *6*, 105948.
- [56] H. Souzandeh, K. S. Johnson, Y. Wang, K. Bhamidipaty, W.-H. Zhong, *ACS Appl. Mater. Interfaces* **2016**, *8*, 20023.
- [57] M. Zhu, Q. Cao, B. Liu, H. Guo, X. Wang, Y. Han, G. Sun, Y. Li, J. Zhou, *Cellulose* **2020**, *27*, 3889.
- [58] C. Wang, S. Wu, M. Jian, J. Xie, L. Xu, X. Yang, Q. Zheng, Y. Zhang, *Nano Res.* **2016**, *9*, 2590.
- [59] K. Min, S. Kim, S. Kim, *Sci. Rep.* **2018**, *8*, 9598.
- [60] Y. Li, L. Cao, X. Yin, Y. Si, J. Yu, B. Ding, *J. Colloid Interface Sci.* **2020**, *578*, 565.
- [61] A. Rajak, D. A. Hapidin, F. Iskandar, M. M. Munir, K. Khairurrijal, *Waste Manag.* **2020**, *103*, 76.
- [62] M. S. Islam, B. C. Ang, A. Andriyana, A. M. Afifi, *SN Appl. Sci.* **2019**, *1*, 1248.
- [63] X. Wang, H. Xiang, C. Song, D. Zhu, J. Sui, Q. Liu, Y. Long, *J. Hazard. Mater.* **2020**, *385*, 121535.
- [64] X. Yang, Y. Pu, Y. Zhang, X. Liu, J. Li, D. Yuan, X. Ning, *J. Hazard. Mater.* **2020**, *391*, 122254.
- [65] D. Ruan, L. Qin, R. Chen, G. Xu, Z. Su, J. Cheng, S. Xie, F. Cheng, F. Ko, *Nanoscale Res. Lett.* **2020**, *15*, 7.
- [66] Y. Guo, W. He, J. Liu, J. Appl. Polym. Sci. **2020**, *137*, 48282.
- [67] A. Vanangamudi, S. Hamzah, G. Singh, *Chem. Eng. J.* **2015**, *260*, 801.
- [68] F. Liu, M. Li, F. Li, K. Weng, K. Qi, C. Liu, Q. Ni, X. Tao, J. Zhang, W. Shao, J. He, *Macromol. Mater. Eng.* **2020**, *305*, 1900856.
- [69] X. Zhao, Y. Li, T. Hua, P. Jiang, X. Yin, J. Yu, B. Ding, *ACS Appl. Mater. Interfaces* **2017**, *9*, 12054.
- [70] J. Li, D. Zhang, T. Yang, S. Yang, X. Yang, H. Zhu, *J. Membr. Sci.* **2018**, *551*, 85.
- [71] G. Nallathambi, B. Robert, S. P. Esmeralda, J. Kumaravel, V. Parthiban, *Res. J. Text. Apparel* **2020**, *24*, 72.
- [72] Q. Wang, O. Yildiz, A. Li, K. Aly, Y. Qiu, Q. Jiang, D. Y. Pui, S.-C. Chen, P. D. Bradford, *Sep. Purif. Technol.* **2020**, *236*, 116255.
- [73] N. Kobayashi, H. Izumi, Y. Morimoto, *J. Occup. Health* **2017**, *59*, 394.
- [74] Z. Wang, Y. Zhang, X. Y. D. Ma, J. Ang, Z. Zeng, B. F. Ng, M. P. Wan, S.-C. Wong, X. Lu, *Sep. Purif. Technol.* **2020**, *235*, 116183.
- [75] M. Hu, L. Yin, N. Low, D. Ji, Y. Liu, J. Yao, Z. Zhong, W. Xing, *J. Membr. Sci.* **2020**, *594*, 117467.
- [76] E. des Ligneris, L. F. Dumée, R. Al-Attabi, E. Castanet, J. Schütz, L. Kong, *Membranes* **2019**, *9*, 87.
- [77] W. J. Lee, J. Lee, M. H. Kim, L. E. Aguilar, C. H. Park, C. S. Kim, *J. Nanosci. Nanotechnol.* **2019**, *19*, 697.
- [78] A. Tolosa, B. Krüner, N. Jäckel, M. Aslan, C. Vakifahmetoglu, V. Presser, *J. Power Sources* **2016**, *313*, 178.
- [79] A. A. Nada, M. F. Bekheet, R. Viter, P. Miele, S. Roualdes, M. Bechelany, *Appl. Catal., B* **2019**, *251*, 76.
- [80] Q. Zhu, X. Tang, S. Feng, Z. Zhong, J. Yao, Z. Yao, *J. Membr. Sci.* **2019**, *581*, 252.
- [81] B. Wang, Q. Wang, Y. Wang, J. Di, S. Miao, J. Yu, *ACS Appl. Mater. Interfaces* **2019**, *11*, 43409.
- [82] Y. Wang, S. Zhan, S. Di, X. Zhao, *ACS Appl. Mater. Interfaces* **2018**, *10*, 26396.
- [83] P. Zhang, S. Zhang, D. Wan, P. Zhang, Z. Zhang, G. Shao, *J. Hazard. Mater.* **2020**, *395*, 122639.
- [84] M.-W. Kim, S. An, H. Seok, A. L. Yarin, S. S. Yoon, *ACS Appl. Mater. Interfaces* **2020**, *12*, 25266.
- [85] M.-W. Kim, S. An, H. Seok, S. S. Yoon, A. L. Yarin, *ACS Appl. Mater. Interfaces* **2019**, *11*, 26323.
- [86] B. Raghavan, H. Soto, K. Lozano, *J. Eng. Fibers Fabr.* **2013**, *8*, 52.
- [87] X. Hao, Y. Zeng, *Ind. Eng. Chem. Res.* **2019**, *58*, 11624.
- [88] M. A. Hassan, B. Y. Yeom, A. Wilkie, B. Pourdeyhimi, S. A. Khan, *J. Membr. Sci.* **2013**, *427*, 336.
- [89] M. A. Hassan, S. A. Khan, B. Pourdeyhimi, *J Appl Polym Sci* **2016**, *133*, 42998.

- [90] A. Brochocka, A. Nowak, K. Majchrzycka, M. Puchalski, S. Sztajnowski, *Materials* **2020**, *13*, 712.
- [91] N. Deng, H. He, J. Yan, Y. Zhao, E. Ben Ticha, Y. Liu, W. Kang, B. Cheng, *Polymer* **2019**, *165*, 174.
- [92] H. Zhang, Q. Zhen, Y. Liu, R. Liu, Y. Zhang, *Results Phys.* **2019**, *12*, 1421.
- [93] J. Zhang, G. Chen, G. S. Bhat, H. Azari, H. Pen, *J. Appl. Polym. Sci.* **2020**, *137*, 48309.
- [94] T. Nakajima, K. Kajiwara, J. E. McIntyre, *Advanced Fiber Spinning Technology*, Woodhead Publishing Limited, Cambridge **2009**.
- [95] X. Zhu, Z. Dai, K. Xu, Y. Zhao, Q. Ke, *Macromol. Mater. Eng.* **2019**, *304*, 1900350.
- [96] H. Zhang, J. Liu, X. Zhang, C. Huang, X. Jin, *RSC Adv.* **2018**, *8*, 7932.
- [97] T.-T. Li, X. Cen, H.-T. Ren, L. Wu, H.-K. Peng, W. Wang, B. Gao, C.-W. Lou, J.-H. Lin, *ACS Appl. Mater. Interfaces* **2020**, *12*, 8730.
- [98] E. S. Medeiros, G. M. Glenn, A. P. Klamczynski, W. J. Orts, L. H. C. Mattoso, *J. Appl. Polym. Sci.* **2009**, *113*, 2322.
- [99] J. L. Daristotle, A. M. Behrens, A. D. Sandler, P. Kofinas, *ACS Appl. Mater. Interfaces* **2016**, *8*, 34951.
- [100] S. Sett, K. Stephansen, A. L. Yarin, *Polymer* **2016**, *93*, 78.
- [101] N. P. B. Tan, S. S. Paclijan, H. N. M. Ali, C. M. J. S. Hallazgo, C. J. F. Lopez, Y. C. Ebor, *ACS Appl. Nano Mater.* **2019**, *2*, 2475.
- [102] L. Shi, X. Zhuang, X. Tao, B. Cheng, W. Kang, *Fibers Polym.* **2013**, *14*, 1485.
- [103] B. Khalid, X. Bai, H. Wei, Y. Huang, H. Wu, Y. Cui, *Nano Lett.* **2017**, *17*, 1140.
- [104] Z. Li, J. Song, Y. Long, C. Jia, Z. Liu, L. Li, C. Yang, J. Liu, S. Lin, H. Wang, Y. Liu, M. Fang, H. Wu, *Nano Res.* **2020**, *13*, 861.
- [105] H. Wang, S. Lin, S. Yang, X. Yang, J. Song, D. Wang, H. Wang, Z. Liu, B. Li, M. Fang, N. Wang, H. Wu, *Small* **2018**, *14*, e1800258.
- [106] S. K. Batra, B. Pourdeyimi, *Introduction to Nonwovens Technology*, Destech Publications, Lancaster **2012**.
- [107] D. V. Rosato, M. G. Rosato, *Concise Encyclopedia of Plastics*, Springer, New York **2000**.
- [108] M. Kamiyama, T. Soeda, S. Nagajima, K. Tanaka, *Polym. J.* **2012**, *44*, 987.
- [109] X. Zhang, Y. Lu, *Polym. Rev.* **2014**, *54*, 677.
- [110] X. Liu, B. Cao, P. Li, *Ind. Eng. Chem. Res.* **2018**, *57*, 329.
- [111] L.-Y. Wang, L. E. Yu, T.-S. Chung, *J. Membr. Sci.* **2020**, *595*, 117561.
- [112] T. Sparks, *Filters and Filtration Handbook*, Elsevier, Boston **2015**.
- [113] K. Thangadurai, G. Thilagavathi, A. Bhattacharyya, *J. Text. I.* **2014**, *105*, 1319.
- [114] D. Moyo, A. Patanaik, R. D. Anandjiwala, in *Process Control in Textile Manufacturing*, Woodhead Publishing Limited **2013**, p. 279.
- [115] R. Roy, S. M. Ishtiaque, *Fibers Polym.* **2020**, *21*, 2125.
- [116] S. Debnath, V. K. Chauhan, J. P. Singh, *J. Text. I.* **2020**, *111*, 1159.
- [117] R. Roy, S. Chatterjee, *Fibers Polym.* **2018**, *19*, 2597.
- [118] S. Sakthivel, A. J. Ezhil, T. Ramachandran, *J. Eng. Fibers Fabr.* **2014**, *9*, 149.
- [119] K. Xu, J. Deng, R. Lin, H. Zhang, Q. Ke, C. Huang, *J. Mater. Chem. A* **2020**, *8*, 22269.
- [120] S. Ma, M. Zhang, J. Nie, J. Tan, B. Yang, S. Song, *Carbohydr. Polym.* **2019**, *203*, 415.
- [121] S. Ma, M. Zhang, J. Nie, B. Yang, S. Song, P. Lu, *Cellulose* **2018**, *25*, 5999.
- [122] Y. Zhang, Z. Zeng, X. Y. D. Ma, C. Zhao, J. M. Ang, B. F. Ng, M. P. Wan, S.-C. Wong, Z. Wang, X. Lu, *Appl. Surf. Sci.* **2019**, *479*, 700.
- [123] F. Deuber, S. Mousavi, L. Federer, M. Hofer, C. Adhart, *ACS Appl. Mater. Interfaces* **2018**, *10*, 9069.
- [124] W.-R. Huang, Z. He, J.-L. Wang, J.-W. Liu, S.-H. Yu, *iScience* **2019**, *12*, 333.
- [125] S. Jeong, H. Cho, S. Han, P. Won, H. Lee, S. Hong, J. Yeo, J. Kwon, S. H. Ko, *Nano letters* **2017**, *17*, 4339.
- [126] D. Y. Choi, K. J. Heo, J. Kang, E. J. An, S.-H. Jung, B. U. Lee, H. M. Lee, J. H. Jung, *J. Hazard. Mater.* **2018**, *351*, 29.
- [127] D. Y. Choi, S.-H. Jung, D. K. Song, E. J. An, D. Park, T.-O. Kim, J. H. Jung, H. M. Lee, *ACS Appl. Mater. Interfaces* **2017**, *9*, 16495.
- [128] R.-Y. Zhang, G.-W. Hsieh, *Environ. Sci.: Nano* **2020**, *7*, 3303.
- [129] W. Zou, B. Gu, S. Sun, S. Wang, X. Li, H. Zhao, P. Yang, *Mater. Res. Express* **2019**, *6*, 105624.
- [130] S. B. Jeong, K. J. Heo, B. U. Lee, *Int. J. Environ. Res. Public Health* **2020**, *17*, 190.
- [131] X. Fan, Y. Wang, L. Kong, X. Fu, M. Zheng, T. Liu, W.-H. Zhong, S. Pan, *ACS Sustainable Chem. Eng.* **2018**, *6*, 11606.
- [132] C. Balagna, S. Perero, F. Bosco, C. Mollea, M. Irfan, M. Ferraris, *Appl. Surf. Sci.* **2020**, *508*, 145283.
- [133] W. Wang, X. Hu, L. Li, W. Jing, A. Guo, H. Du, *Ceram. Int.* **2019**, *45*, 6723.
- [134] Q. Liu, T. Xue, L. Yang, X. Hu, H. Du, *J. Eur. Ceram. Soc.* **2016**, *36*, 1691.
- [135] Z. Cuo, H. Liu, F. Zhao, W. Li, S. Peng, Y. Chen, *Ceram. Int.* **2018**, *44*, 11778.
- [136] Z. Cuo, J. Zhang, B. Yu, S. Peng, H. Liu, Y. Chen, *Sep. Purif. Technol.* **2019**, *215*, 368.
- [137] M. D. d. M. Innocentini, J. R. Coury, M. Fukushima, P. Colombo, *Sep. Purif. Technol.* **2015**, *152*, 180.
- [138] M. Adam, C. Vakifahmetoglu, P. Colombo, M. Wilhelm, G. Grathwohl, *J. Am. Ceram. Soc.* **2014**, *97*, 959.
- [139] C. Vakifahmetoglu, P. Colombo, S. M. Carturan, E. Pippel, J. Woltersdorf, *J. Am. Ceram. Soc.* **2010**, *93*, 3709.
- [140] C. Vakifahmetoglu, E. Pippel, J. Woltersdorf, P. Colombo, *J. Am. Ceram. Soc.* **2010**, *93*, 959.
- [141] K.-T. Park, J. Hwang, *Carbon* **2014**, *75*, 401.
- [142] J. Park, J. Jeong, C. Kim, J. Hwang, *Aerosol Sci. Technol.* **2013**, *47*, 512.
- [143] A. Gili, L. Schlicker, M. F. Bekheet, O. Görke, S. Penner, M. Grünbacher, T. Götsch, P. Littlewood, T. J. Marks, P. C. Stair, R. Schomäcker, A. Doran, S. Selve, U. Simon, A. Gurlo, *ACS Catal.* **2018**, *8*, 8739.
- [144] A. Gili, L. Schlicker, M. F. Bekheet, O. Görke, D. Kober, U. Simon, P. Littlewood, R. Schomäcker, A. Doran, D. Gaissmaier, T. Jacob, S. Selve, A. Gurlo, *ACS Catal.* **2019**, *9*, 6999.
- [145] P. Li, C. Wang, Z. Li, Y. Zong, Y. Zhang, X. Yang, S. Li, F. Wei, *RSC Adv* **2014**, *4*, 54115.
- [146] P. Li, Y. Zong, Y. Zhang, M. Yang, R. Zhang, S. Li, F. Wei, *Nanoscale* **2013**, *5*, 3367.
- [147] J. H. Park, K. Y. Yoon, H. Na, Y. S. Kim, J. Hwang, J. Kim, Y. H. Yoon, *Sci. Total Environ.* **2011**, *409*, 4132.
- [148] Y. Zhao, Z.-X. Low, S. Feng, Z. Zhong, Y. Wang, Z. Yao, *Nanoscale* **2017**, *9*, 5433.
- [149] Y. Zhao, Z. Zhong, Z.-X. Low, Z. Yao, *RSC Adv.* **2015**, *5*, 91951.
- [150] C. Xu, W. Xie, Y. Yu, J. Zhang, J. Yang, *Mater. Res. Express* **2019**, *6*, 25024.
- [151] H. Parham, S. Bates, Y. Xia, Y. Zhu, *Carbon* **2013**, *54*, 215.
- [152] S. Yang, Z. Zhu, F. Wei, X. Yang, *Build. Environ.* **2017**, *125*, 60.
- [153] K. Yang, Z. Yu, C. Yu, H. Chen, F. Pan, *Adv. Mater. Technol.* **2019**, *4*, 1900101.
- [154] A. G. Nasibulin, A. Kaskela, K. Mustonen, A. S. Anisimov, V. Ruiz, S. Kivistö, S. Rackauskas, M. Y. Timmermans, M. Pudas, B. Aitchison, M. Kauppinen, D. P. Brown, O. G. Okhotnikov, E. I. Kauppinen, *ACS Nano* **2011**, *5*, 3214.
- [155] E. Aram, S. Mehdipour-Ataei, *Int. J. Polym. Mater. Polym. Biomater.* **2016**, *65*, 358.
- [156] C. Vakifahmetoglu, *Ceram. Int.* **2014**, *40*, 11925.
- [157] T. Semerci, M. D. de Mello Innocentini, G. A. Marsola, P. R. O. Lasso, G. D. Soraru, C. Vakifahmetoglu, *ACS Appl. Polym. Mater.* **2020**, *2*, 4118.

- [158] C. Vakifahmetoglu, D. Zeydanli, V. C. Ozalp, B. A. Borsa, G. D. Soraru, *Mater. Des.* **2018**, *140*, 37.
- [159] A. Karakuscu, A. Ponzoni, E. Comini, G. Sberveglieri, C. Vakifahmetoglu, *Int. J. Appl. Ceram. Technol.* **2014**, *11*, 851.
- [160] E. B. Ertuş, C. Vakifahmetoglu, A. Öztürk, *Ceram. Int.* **2020**, *46*, 4947.
- [161] L. M. Henning, D. D. Cubas, M. G. Colmenares, J. Schmidt, M. F. Bekheet, B. R. Pauw, A. Gurlo, U. Simon, *Micropor. Mesopor. Mat.* **2019**, *280*, 133.
- [162] X. Wang, F. Schmidt, D. Hanaor, P. H. Kamm, S. Li, A. Gurlo, *Addit. Manuf.* **2019**, *27*, 80.
- [163] M. G. Colmenares, U. Simon, F. Schmidt, S. Dey, J. Schmidt, A. Thomas, A. Gurlo, *Micropor. Mesopor. Mat.* **2018**, *267*, 142.
- [164] F. Zemke, V. Schölch, M. F. Bekheet, F. Schmidt, *Nanomater. Energy* **2019**, *8*, 126.
- [165] A. Gili, B. Bischoff, U. Simon, F. Schmidt, D. Kober, O. Görke, M. F. Bekheet, A. Gurlo, *Membranes* **2019**, *9*, 108.
- [166] C. Vakifahmetoglu, M. Buldu, A. Karakuscu, A. Ponzoni, D. Assefa, G. D. Soraru, *J. Eur. Ceram. Soc.* **2015**, *35*, 4447.
- [167] S.-J. Choi, K. Kim, H. Kim, J. Yoon, M. Lee, K.-S. Choi, U.-D. Sung, W.-T. Park, J. Lee, J. Jeon, J. Im, K.-K. Kim, S. Cho, *Appl. Sci.* **2019**, *9*, 235.
- [168] M. Briffa, S. Decelis, J.-P. Brincat, J. N. Grima, R. Gatt, V. Valdramidis, *Food Control* **2017**, *73*, 91.
- [169] M. Taylor, B. McCollister, D. Park, *Appl. Biochem. Biotechnol.* **2016**, *178*, 1053.
- [170] Y. Wang, W.-L. Yuan, L. Zhang, Z. Zhang, G.-H. Zhang, S.-L. Wang, L. He, G.-H. Tao, *Adv. Sustainable Syst.* **2020**, *8*, 2000046.
- [171] G. Ramya, B. Crittenden, M. Smith, O. Camus, Y. J. Chew, S. Perera, *Chem. Eng. J.* **2019**, *361*, 736.
- [172] G. Ramya, O. Camus, Y. M. J. Chew, B. Crittenden, S. Perera, *ACS Appl. Polym. Mater.* **2020**, *2*, 1569.
- [173] Z. Li, J. Xu, D. Sun, T. Lin, F. Huang, *ACS Appl. Nano Mater.* **2020**, *3*, 1564.
- [174] H. Maleki, *Chem. Eng. J.* **2016**, *300*, 98.
- [175] D. Assefa, E. Zera, R. Camprostrini, G. D. Soraru, C. Vakifahmetoglu, *Ceram. Int.* **2016**, *42*, 11805.
- [176] G. Shao, D. A. H. Hanaor, J. Wang, D. Kober, S. Li, X. Wang, X. Shen, M. F. Bekheet, A. Gurlo, *ACS Appl. Mater. Interfaces* **2020**, *12*, 46045.
- [177] G. Shao, O. Ovsianyskyi, M. F. Bekheet, A. Gurlo, *Chem. Commun.* **2020**, *56*, 450.
- [178] Y. Wang, X. Chen, Y. Kuang, M. Xiao, Y. Su, F. Jiang, *Int. J. Low-Carbon Technol.* **2019**, *14*, 335.
- [179] J. Nemoto, T. Saito, A. Isogai, *ACS Appl. Mater. Interfaces* **2015**, *7*, 19809.
- [180] Y. Xie, F. Guo, J. Mao, J. Huang, Z. Chen, Y. Jiang, Y. Lai, *Sep. Purif. Technol.* **2021**, *254*, 117571.
- [181] S. J. Kim, G. Chase, S. C. Jana, *Sep. Purif. Technol.* **2015**, *156*, 803.
- [182] C. Zhai, S. C. Jana, *ACS Appl. Mater. Interfaces* **2017**, *9*, 30074.
- [183] K. Zhao, J. Huang, J. Mao, Z. Bao, Z. Chen, Y. Lai, *Chem. Eng. J.* **2020**, *395*, 125086.
- [184] Y.-G. Zhang, Y.-J. Zhu, Z.-C. Xiong, J. Wu, F. Chen, *ACS Appl. Mater. Interfaces* **2018**, *10*, 13019.
- [185] W. Jung, J. S. Lee, S. Han, S. H. Ko, T. Kim, Y. H. Kim, *J. Mater. Chem. A* **2018**, *6*, 16975.
- [186] W. Jung, M. H. Jeong, K. H. Ahn, T. Kim, Y. H. Kim, *J. Hazard. Mater.* **2020**, *391*, 122223.
- [187] H.-J. Yoon, D.-H. Kim, W. Seung, U. Khan, T. Y. Kim, T. Kim, S.-W. Kim, *Nano Energy* **2019**, *63*, 103857.
- [188] X. Xu, S. Xiao, H. J. Willy, T. Xiong, R. Borayek, W. Chen, D. Zhang, J. Ding, *Appl. Catal., B* **2020**, *262*, 118307.
- [189] T. Kozior, A. Mamun, M. Trabelsi, M. Wortmann, S. Lilia, A. Ehrmann, *Polymers* **2019**, *11*, 2034.
- [190] X. Wang, F. Schmidt, A. Gurlo, *J. Eur. Ceram. Soc.* **2020**, *40*, 315.
- [191] A. Bahrami, U. Simon, N. Soltani, S. Zavareh, J. Schmidt, M. I. Pech-Canul, A. Gurlo, *Green Chem.* **2017**, *19*, 188.
- [192] L. M. Henning, S. Zavareh, P. H. Kamm, M. Höner, H. Fischer, J. Banhart, F. Schmidt, A. Gurlo, *Adv. Eng. Mater.* **2017**, *19*, 1700129.
- [193] A. Abdullayev, P. H. Kamm, M. F. Bekheet, A. Gurlo, *Membranes* **2020**, *10*, 93.
- [194] N. Soltani, U. Simon, A. Bahrami, X. Wang, S. Selve, J. D. Epping, M. I. Pech-Canul, M. F. Bekheet, A. Gurlo, *J. Eur. Ceram. Soc.* **2017**, *37*, 4809.
- [195] Z. Zeng, X. Y. D. Ma, Y. Zhang, Z. Wang, B. F. Ng, M. P. Wan, X. Lu, *ACS Sustainable Chem. Eng.* **2019**, *7*, 6959.
- [196] T. Fukasawa, M. Ando, T. Ohji, *J. Ceram. Soc. Jpn.* **2002**, *110*, 627.
- [197] B. K. Kaang, H. B. Lee, H. Y. Koo, W. S. Choi, *ACS Sustainable Chem. Eng.* **2020**, *8*, 13984.
- [198] N. Bader, U. Sager, U. Schneiderwind, A. Ouederni, *J. Environ. Chem. Eng.* **2019**, *7*, 103005.
- [199] Y.-C. Chen, C.-H. Liao, W.-T. Shen, C. Su, Y.-C. Wu, M.-H. Tsai, S.-S. Hsiao, K.-P. Yu, C.-H. Tseng, *Indoor air* **2019**, *29*, 439.
- [200] A. Dey, N. Kayal, O. Chakrabarti, R. F. Caldato, M. D. d. M. Innocentini, V. G. Guerra, *Int. J. Appl. Ceram. Technol.* **2014**, *11*, 804.
- [201] A. Dey, N. Kayal, O. Chakrabarti, R. F. Caldato, C. M. André, M. D. M. Innocentini, *Ind. Eng. Chem. Res.* **2013**, *52*, 18362.
- [202] A. Abdullayev, M. F. Bekheet, D. A. H. Hanaor, A. Gurlo, *Membranes* **2019**, *9*, 105.
- [203] S.-K. Ryi, J.-S. Park, S.-J. Park, D.-G. Lee, S.-H. Kim, *J. Membr. Sci.* **2007**, *299*, 174.
- [204] W. Wei, W. Zhang, Q. Jiang, P. Xu, Z. Zhong, F. Zhang, W. Xing, *J. Membr. Sci.* **2017**, *540*, 381.
- [205] C.-C. Ho, F. Kang, G.-M. Chang, S.-J. You, Y.-F. Wang, *Appl. Surf. Sci.* **2019**, *465*, 31.
- [206] X. Zhao, S. Wang, X. Yin, J. Yu, B. Ding, *Sci. Rep.* **2016**, *6*, 35472.
- [207] K. M. Yun, A. B. Suryamas, F. Iskandar, L. Bao, H. Niinuma, K. Okuyama, *Sep. Purif. Technol.* **2010**, *75*, 340.
- [208] L. Bao, K. Seki, H. Niinuma, Y. Otani, R. Balgis, T. Ogi, L. Gradon, K. Okuyama, *Sep. Purif. Technol.* **2016**, *159*, 100.
- [209] C. Vakifahmetoglu, D. Zeydanli, M. D. d. M. Innocentini, F. D. S. Ribeiro, P. R. O. Lasso, G. D. Soraru, *Sci. Rep.* **2017**, *7*, 41049.
- [210] Y.-M. Kuo, S.-H. Huang, W.-Y. Lin, M.-F. Hsiao, C.-C. Chen, *J. Aerosol Sci.* **2010**, *41*, 223.
- [211] S.-R. Tian, G.-H. Yang, Z. Li, K.-Y. Shi, G.-Z. Ding, F.-X. Hu, *Powder Technol.* **2016**, *301*, 545.
- [212] J. Xu, C. Liu, P.-C. Hsu, K. Liu, R. Zhang, Y. Liu, Y. Cui, *Nano Lett.* **2016**, *16*, 1270.
- [213] P. P. Tsai, H. Schreuder-Gibson, P. Gibson, *J. Electrostat.* **2002**, *54*, 333.
- [214] Y. Bai, C. B. Han, C. He, G. Q. Gu, J. H. Nie, J. J. Shao, T. X. Xiao, C. R. Deng, Z. L. Wang, *Adv. Funct. Mater.* **2018**, *28*, 1706680.
- [215] X. Zhao, Y. Li, T. Hua, P. Jiang, X. Yin, J. Yu, B. Ding, *Small* **2017**, *13*, 1603306.
- [216] A. Al-Jumaili, S. Alancherry, K. Bazaka, M. V. Jacob, *Materials* **2017**, *10*, 1066.
- [217] C. Wang, S. Lu, Z. Zhang, *Sci. Total Environ.* **2019**, *655*, 787.
- [218] P. Li, J. Li, X. Feng, J. Li, Y. Hao, J. Zhang, H. Wang, A. Yin, J. Zhou, X. Ma, B. Wang, *Nat. Commun.* **2019**, *10*, 2177.
- [219] E. Horváth, L. Rossi, C. Mercier, C. Lehmann, A. Sienkiewicz, L. Forró, *Adv. Funct. Mater.* **2020**, *30*, 2004615.

- [220] V. Kadam, I. L. Kyratzis, Y. B. Truong, L. Wang, R. Padhye, *J. Appl. Polym. Sci.* **2020**, 137, 49228.
- [221] Z. Xu, *Fundamentals of Air Cleaning Technology and Its Application in Cleanrooms*, Springer, Berlin **2014**.
- [222] A. Simmons, S. Lerouge, *Sterilisation of Biomaterials and Medical Devices: Methods, Analysis and Applications*, Woodhead Publishing, Cambridge **2012**.
- [223] L. Liao, W. Xiao, M. Zhao, X. Yu, H. Wang, Q. Wang, S. Chu, Y. Cui, *ACS Nano* **2020**, 14, 6348.
- [224] P. Anastas, N. Eghbali, *Chem. Soc. Rev.* **2010**, 39, 301.
- [225] R. Krause, T. Oppelt, C. Friebe, S. Döge, R. Herzog, *MATEC Web Conf.* **2020**, 324, 3002.
- [226] J. Mo, C. Zhang, Y. Lu, Y. Liu, N. Zhang, S. Wang, S. Nie, *Nano Energy* **2020**, 78, 105357.
- [227] A. Raghunath, E. Perumal, *Int. J. Antimicrob. Agents* **2017**, 49, 137.
- [228] T. Xia, Y. Bian, L. Zhang, C. Chen, *Energy Build.* **2018**, 158, 987.
- [229] J. Serode, Sustainable Facade for Improved Air Quality, ECE Projektmanagement GmbH, **2020**, <https://www.ece.com/en/company/sustainability/sustainable-facade> (accessed: December 2020).
- [230] W. C. Hinds, *Aerosol Technology: Properties, Behavior, and Measurement of Airborne Particles*, Wiley-Interscience, New York **2012**.
- [231] C. Vakifahmetoglu, *Adv. Appl. Ceram.* **2011**, 110, 188.



Laura M. Henning obtained her M.Sc. in materials science from Technische Universität Berlin (Germany), in 2018. Presently, she is a Ph.D. student at the Chair of Advanced Ceramic Materials, Technische Universität Berlin, under supervision of Prof. Dr. Aleksander Gurlo. Her current research interest is focused on the synthesis, processing, and surface functionalization of porous ceramic materials for environmental applications, particularly the management of wastewater and air pollution using adsorption and filtration processes.



Amanmyrat Abdullayev obtained his diploma in environmental studies from Magtumguly Turkmen State University (Turkmenistan) in 2014. Currently, he is a Ph.D. student at the Chair of Advanced Ceramic Materials, Technische Universität Berlin, under the supervision of Prof. Aleksander Gurlo. His research interests are the fabrication and application of porous ceramic materials for environmental remediation purposes, specifically the treatment of wastewater using low-cost natural resources.



Cekdar Vakifahmetoglu, after completing his Ph.D. on porous ceramics with Prof. Ing. Paolo Colombo (University of Padova, Italy), he joined the group of Prof. Dr. Richard E. Riman (Rutgers, NJ, USA) as a postdoc to work on hydro and solvothermal methods for solution crystallization and for densification of inorganic solids at low temperatures. His current research is devoted mainly to (i) additive manufacturing of metals, inorganics and composite systems, (ii) green & low-energy manufacturing, utilization of waste/recycled materials, (iii) processing and applications of polymer derived ceramics, and porous materials in particular foams and aerogels.



Ulla Simon obtained her Ph.D. in materials science in the field of heterogenous catalysis from Technische Universität Berlin (Germany), in 2014. Since 2015, she has been working as a lecturer and research group leader at the Chair of Advanced Ceramic Materials at Technische Universität Berlin. Her main research fields are the synthesis, characterization, and processing of functional oxide ceramics and porous materials for heterogenous catalysis, adsorption and biomaterials.



Hiba Bensalah completed her Ph.D. in chemical engineering in December 2019, under the supervision of Prof. Dr. Aleksander Gurlo, at the Chair of Advanced Ceramic Materials at Technische Universität Berlin (Germany). Since then, she has been working as a postdoctoral researcher at the same chair. Her main research interest is water and wastewater treatment, filtration techniques such as membrane processes and adsorption, industrial waste management. Currently, she is exploring the use of new technologies in water treatment: AM and computational fluid dynamics (CFD) for the improvement of membranes performances.



Aleksander Gurlo obtained his Ph.D. in chemistry from the Belarusian State University (Minsk, Belarus) in 1998 and his habilitation in materials science, in 2010, from the Technische Universität Darmstadt (Germany). Since 2014, he has been a full professor at Chair of Advanced Ceramic Materials at Technische Universität Berlin. His research focus is on advanced ceramics, with emphasis on the design, synthesis, and characterization of various ceramic materials, the development of fabrication techniques and in situ/in operando characterization of materials properties and formation.



Maged F. Bekheet obtained his Ph.D. in material science and engineering with distinction from Technische Universität Darmstadt (Germany), in 2014. Since 2014, he has been working as a lecturer and research group leader at the Chair of Advanced Ceramic Materials at Technische Universität Berlin (Germany). His current research interest is focused on the design, synthesis, and ex situ and in situ/operando characterization of different functional material classes for catalysis and membranes, gas sensing, energy, and environmental applications.